JARO 9: 44–64 (2008)
DOI: 10.1007/s10162-007-0105-8

JARO
Journal of the Association for Research in Otolaryngology

Rapid Hair Cell Loss: A Mouse Model for Cochlear Lesions

Ruth Rebecca Taylor, Graham Nevill, and Andrew Forge

[1] *Centre for Auditory Research, UCL Ear Institute, University College London, 332 Gray's Inn Road, London, WC1X 8EE, UK*

Received: 26 June 2007; Accepted: 25 October 2007; Online publication: 4 December 2007

ABSTRACT

In comparison to other mammals, mice have proved extremely resistant to aminoglycoside-induced hair cell ablation in vivo. In this paper we examine the pattern and extent of cochlear lesions rapidly induced with a combination of a single dose of aminoglycoside (kanamycin) followed by a loop diuretic (bumetanide). With this protocol, the vestibular system was unaffected, but in the cochlea, there was extensive loss of outer hair cells (OHC) that commenced in the basal coil and progressed apically so that, by 48 h, OHC loss was almost complete. TUNEL-positive nuclei and activated caspase-3 labeling demonstrated that most OHC died via a classical apoptotic pathway. However, scattered debris within the OHC region suggested that many apoptotic cells ruptured prior to completion of apoptosis. Following lesion repair, supporting cells retained characteristics of differentiated cells but positional shift occurred. In comparison to OHC loss, inner hair cell (IHC) death was delayed and only observed in 50% of all cochleae examined even after extensive reorganization of the tissue. The coadmininstration of diuretic with FM1-43, used as a tracer for aminoglycoside uptake, indicated entry into IHC as readily as OHC, suggesting that the differential response to aminoglycoside was not due to differential uptake. Where IHC death was ongoing, there were indications of different modes of cell death: cells with morphological features of autophagy, necrosis, and apoptosis were apparent. In addition to damage to the organ of Corti, there was a significant and progressive decrease in strial thickness beginning as early as 7 days posttreatment. This was due predominantly to degeneration of marginal cells. The strial pathology resembled that reported after noise damage and with aging. This in vivo protocol provides a robust model in which to obtain extensive OHC loss in the mature cochleae of mice and is a means with which to examine different aspects of cochlear pathology in transgenic or mutant strains.

Keywords: aminoglycoside, diuretic, hair cell death, autophagy, stria vascularis, FM1-43

INTRODUCTION

The ability to manipulate the genome, and the existence of many naturally occurring mutants with auditory phenotypes that have corollaries in humans, has made the mouse the animal of choice for a variety of studies of the auditory system. Mice are thus of potential value in investigation of the molecular basis of cochlear pathologies and of the possibilities for therapeutic interventions aimed at preventing deafness or at regenerating hair cells as a means to restore hearing. Such investigations require models of cochlear injury and of induced hair cell loss with which to explore the underlying basic mechanisms. The ototoxic action of aminoglycosides, in addition to its clinical significance as a major causative factor in the incidence of acquired hearing loss and balance dysfunction throughout the world, also provides a more general model of mechanisms of injury to the cochlea. In particular, the basis of hair cell death, and of how the cochlea responds to such damage, can be explored (Forge and Schacht 2000). However, it has proved remarkably difficult to induce hair cell loss in vivo in the mature cochleae of mice as easily as can be achieved in other animal models such as guinea pigs. It seems that very high doses of aminoglycoside need to be administered to mice before any ototoxicity is evident (Wu et al. 2001). With many aminoglycosides, including gentamicin, the aminoglycoside most commonly used in

Correspondence to: Ruth Rebecca Taylor · Centre for Auditory Research, UCL Ear Institute · University College London · 332 Gray's Inn Road, London, WC1X 8EE, UK. Telephone: +44-20-76798954; fax: +44-20-76798990; email: ruth.r.taylor@ucl.ac.uk

experimental studies of ototoxicity, and neomycin, the dosing conditions sufficient to induce hair cell loss in mice could not be determined. At lower doses given repeatedly on successive days, no hair cell loss occurred, but with higher doses, single injections of the drug were rapidly lethal. However, it proved possible to administer high doses of kanamycin. Using twice daily injections of this high dose for 14 days, progressive hair cell loss occurred (Wu et al. 2001). While this regime has certain advantages, the need for so many repeated injections makes this procedure somewhat difficult to employ, especially with large numbers of animals. A combination of a single dose of aminoglycoside closely followed by a single dose of a loop diuretic is known to cause very rapid hair cell loss in humans and experimental animals (West et al. 1973; Russell et al. 1979; Brummett et al. 1981; Webster and Webster 1981). It is a combination recently used in guinea pigs to induce hair cell loss prior to testing a means to induce hair cell regeneration (Izumikawa et al. 2005). Prieve and Yanz (1984) found that kanamycin in combination with bumetanide rapidly induced marked permanent high-frequency threshold shifts in mice. We therefore examined in detail the effects of this combination, using the high doses of kanamycin identified by Wu et al. (2001), upon the cochlea in mice.

METHODS AND MATERIALS

CBA/Ca mice, 18–21 days old, weighing 7–10 g were used. Animals received a single subcutaneous injection of kanamycin (Sigma, St. Louis, MO, USA) dissolved in phosphate-buffered saline (PBS), at 1 mg/g body weight, followed 40 min later by a single intraperitoneal injection of a clinical preparation of the loop diuretic, bumetanide (Burinex, injection, Leo) at 0.05 mg/g. Generally, inner ear tissues were obtained for examination at 24 and 48 h and at 1, 2, and 4 weeks after injections. Some cochleae were obtained at 6 and 18 h after treatment to examine the onset of any effects and others at 8, 12, and 14 weeks posttreatment to explore the longer-term consequences. From any one group of animals injected on the same occasion, treated animals were taken at different time points, usually two animals from each group at each time point. The two ears from any individual animal were prepared for examination by different methods. In total, 156 animals were used. To test for the generality of effects of kanamycin, the use of amikacin at up to 1 mg/g body weight and of gentamicin were examined. The cochleae of these animals were isolated at 7 or 14 days posttreatment. The cochleae of two untreated "aged" CBA/Ca animals, one 12 months old and one 24 months old, were also included in the study. All animal work conformed to the regulated procedures of the British Home Office.

Following its isolation, openings into the cochlea were made by removing a piece of bone covering the apex, rupturing the round window membrane, extracting the stapes from the oval window, and breaking the bone between round and oval windows to give access to the basal cochlear turn and the vestibule. Fixative was perfused directly into the cochlea through these openings. In preparation for immunohistochemistry and fluorescence microscopy of whole mounts and cryosections, tissue was fixed in 4% paraformaldehyde in PBS for 60 min. For electron microscopy, tissue was fixed in 2.5% glutaraldehyde in 0.1 M cacodylate buffer with 3 mM $CaCl_2$ for 2 h at room temperature. Following fixation, cochleae were decalcified in 4.13% EDTA pH 7.3 for 24–48 h at 4°C. Organs of Corti were carefully dissected from the cochleae for whole mount immunohistochemistry and scanning electron microscopy (SEM). Decalcified cochleae were processed and embedded intact prior to thin sectioning for transmission electron microscopy (TEM) or cryosectioning.

Tissue labeling

Whole mounts were rinsed in PBS and permeabilized for 30 min in 0.2% Triton X-100. To identify the pattern and extent of any hair cell loss and concurrent nuclear morphology, the tissue was then incubated in 2 μg/ml phalloidin-flourescein isothiocyanate (FITC), 2 μg/ml propidium iodide, and 100 μg/ml DNAse-free RNase at 37°C for 40 min, or with 2 μg/ml phalloidin conjugated to either FITC or tetramethyl rhodamine iso-thiocyanate alone for 1 h, and nuclei were counterstained with 4′,6-diamidino-2-phenylindole (DAPI). For immunohistochemical labeling, after permeabilization, tissue was incubated at room temperature for 40–60 min in a blocking solution consisting of 5% horse serum and 0.5% bovine serum albumen in PBS with 0.2% Triton X-100. Specimens were washed and incubated overnight at 4°C in primary antibody diluted in PBS with 100 mM lysine and 0.2% Triton X-100. Following several washes, tissue was incubated in appropriate secondary antibodies together with fluorophore-conjugated phalloidin (Sigma). Polyclonal antibody to calretinin (Chemicon, Billerica, MA, USA, 1:200) or monoclonal antibody to parvalbumin (Sigma, 1:200) were used to visualize hair cells in conjunction with phalloidin conjugated to a fluorophore. Polyclonal antibody to rat prestin [gift from JF Ashmore (Weber et al. 2002)] was used to identify outer hair cell (OHC) plasma membranes in some experiments. To identify possible activation of caspase-3 during cell death, tissue was incubated with polyclonal antibody to activated caspase-3 (1:100, Cell Signaling Technology, Danvers, MA, USA). DNA fragmentation, an indicator of apoptosis, was examined by the TUNEL technique using an Apoptag kit with fluorescent (FITC)-conjugated antidigoxigenin antibodies (Chemicon). In

negative controls for antibody labeling, the primary antibody was omitted and undamaged tissue was processed in parallel with damaged tissue in examinations of activated caspase-3 and TUNEL. Samples were mounted in Vectashield containing DAPI (Vector, Burlingame, CA, USA) to counterstain nuclei. The whole mount samples were examined and imaged using either wide-field epifluorescence microscopy on a Zeiss Axioplan with images recorded digitally using a Zeiss Axiocam, or by confocal microscopy on a Zeiss Meta confocal laser scanning microscope. Digital images were exported as TIFF files and adjusted for optimal contrast and brightness.

Preparation for electron microscopy

After the initial fixation in glutaraldehyde, tissue was postfixed in 1% OsO_4 in 0.1 M cacodylate buffer for 90 min. SEM samples were then processed by the thiocarbohydrazide-OsO_4 repeated protocol (Davies and Forge 1987) prior to dehydration through an alcohol series and critical point drying. Samples were sputter coated with gold–palladium or platinum. SEM images were collected digitally. In preparation for thin sectioning, intact, decalcified cochleae were partially dehydrated to 70% ethanol and then incubated in saturated uranyl acetate in 70% ethanol overnight before completing dehydration and embedding in plastic. Sections approximately parallel to the modiolus that included the whole height of the cochlea were taken at five to six successive levels to enable all turns of the cochlear spiral to be examined through the entire depth of the cochlea. At each level, an initial 1-μm-thick section was stained in toluidine blue and examined by light microscopy. A series of thin sections were then cut, at least two of which were collected on formvar-coated single-slot grids to gain uninterrupted views of the section from base to apex. This procedure enabled examination of the entire cochlea, base to apex, and across its whole width, and of the lateral walls and the organ of Corti at the same locations. Thin sections were counterstained in uranyl acetate and lead citrate. Transmission electron micrographs were collected digitally using a Gatan camera. All digital images were formatted with Photoshop v6 (Adobe Systems, San Jose, CA, USA).

Assessment of stria vascularis

Measurements of the thickness of the stria vascularis (SV) were taken from thin sections. At each cochlear turn in each section at each level in each cochlea, three images containing the entire thickness of the SV (endolymphatic surface to interface with spiral ligament) were taken from the central portion of the strial width (along the axis of Reissner's membrane to spiral prominence). Using the Gatan analysis software, measurements of the thickness of the SV, from the endolymphatic surface of marginal cells to the spiral ligament side of basal cells, were obtained from each image. For each cochlea examined, data were pooled to obtain a mean for both basal and apical turns of the cochlea. Measurements of strial thickness were statistically analyzed using Graphpad InStat. One-way ANOVA with Tukey correction was performed.

FM1-43 uptake into hair cells

The uptake of FM1-43 into hair cells in the mature organ of Corti was used to test for possible differences in uptake of drugs into different cell types. For in vitro studies, auditory bullae were isolated from mice aged P18–P21 and the cochlea exposed. Rapidly, and without immersion of the bulla in fluid, the bone covering the apical end of the cochlea and bone between the round and oval windows at the base were removed to provide openings into the cochlea. The bulla with the now opened cochlea was then dropped into 3 μM FM1-43 in 4-2-hydroxyethyl-1-piperazineethanesulfonic acid-buffered Hanks balanced salt solution (Hb-HBSS) that had been equilibrated at 37°C. The cochlea was incubated at 37°C for 10 s before immediate transfer to ice-cold Hb-HBSS, followed by three further washes in Hb-HBSS. Strips of organ of Corti were then isolated, mounted on slides, and immediately examined as whole mounts by wide-field epifluorescence microscopy. Three replicates of this experiment were performed on each of two occasions.

To assess FM1-43 uptake in vivo, mice were injected subcutaneously with 4 μg/g FM1-43 (Meyers et al. 2003) dissolved in PBS. Some animals then received 0.05 mg/g bumetanide by intraperitoneal injection 40 min later. Other animals did not; they received no further treatment. Inner ear tissues were dissected at 2, 6, and 24 h following injection and immediately examined as whole-mount preparations by epifluorescence microscopy. The cochleae from at least three animals at each time point under each condition were examined. Imaging and image recording were performed using the same settings on the microscope and camera system for comparison between animals that had received bumetanide and FM1-43 and those that received only FM1-43. Tissue from animals that received kanamycin rather than FM1-43 with bumetanide acted as controls.

RESULTS

This study was designed to examine the pattern and extent of cochlear lesions induced with a combination of a single dose of aminoglycoside, kanamycin followed by the loop diuretic, bumetanide. Mice that received a

single injection of kanamycin at a dose of 1 mg/g showed no long-lasting systemic effects. Exceeding this dose, however, proved to be toxic, resulting in paralysis, altered breathing patterns, and subsequent death within 20 min (all six animals given 1.25 mg/g died). Following administration of 1 mg/g kanamycin alone, omitting the loop diuretic, no damage to the inner ear was evident at any time point examined; 24 h (n=3), 48 h (n=2), 7 days (n=2), and 14 days (n=2). Likewise, animals that received only the bumetanide showed no adverse effects or cochlear abnormalities at the time points examined [24 h (n=2); 48 h n=1; 7 days n=2]. In contrast, animals that received the combination of kanamycin followed by bumetanide showed an acute response as early as 18 h subsequent to the treatment.

In the cochlea, the kanamycin–bumetanide protocol resulted in virtually complete loss of OHC by 48 h postinjection (effects described in detail below). Phalloidin and DAPI staining of whole mount preparations, SEM, and thin sections revealed that the protocol was effective in 80% of injected mice (194 cochleae out of the 244 examined by these methods). In the remaining 20% of injected animals, no hair cell loss was evident. The cochleae of these animals appeared essentially unaffected. In some animals, during the initial subcutaneous injection of kanamycin, there was leakage

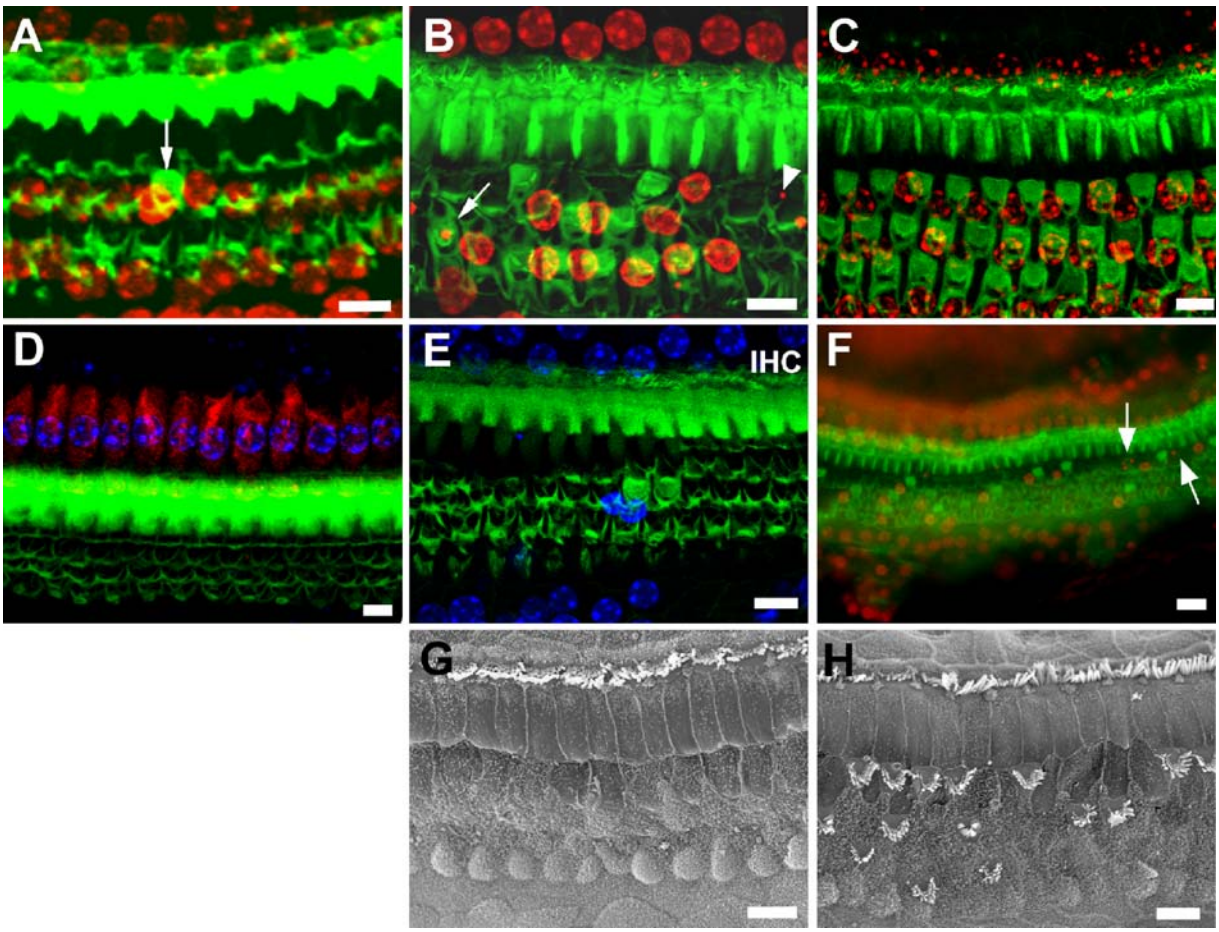

FIG. 1. Progression of OHC loss in the organ of Corti. **A–C** Twenty-four hours posttreatment. **A** Basal turn; **B** middle turn; **C** apical turn. Confocal images of whole mount preparations. Phalloidin-FITC (*green*) labels actin assemblies at the reticular lamina and in hair cells. Nuclei counterstained with DAPI (displayed in *red channel* for greater clarity). **A** In the basal coil, essentially all OHC are lost except for one remaining (*arrow*), whose nucleus shows condensed chromatin. **B** In the middle coil, there is scattered loss of OHC, with the nuclei of remaining ones showing apoptotic features: marginated and condensed chromatin and fragmentation. At the *arrow*, an OHC hair bundle overlies a highly condensed nucleus. *Arrowhead* indicates fragmented nuclei persisting in the absence of any indication of an OHC. **C** In the apical coil, OHC are mainly unaffected. **D–H** Forty-eight hours posttreatment. **D** Basal coil; **E**, **G** middle; **F**, **H** apex. **D**, **E** Confocal image of whole mount preparation; *green*, actin labeled with phalloidin-FITC; *blue*, nuclei counterstained with DAPI; *red* in **D**, calretinin labeling. **F** Wide-field epifluorescence microscopy; *green*, actin; *red*, nuclei counterstained with propidium iodide. **G**, **H** Scanning electron micrographs (SEM). **D** In the basal coil, all OHC are lost and "scars" fill their positions, but all IHC (calretinin positive) are still present. **E** Two remaining OHC; all other OHC are missing. There are no nuclei in the region normally occupied by OHC, but both the apical structures and nuclei of IHC persist. **F** There are scattered persistent OHC, but nuclear fragments (*arrows*) indicate continuing apoptotic death in the apical coil at this time. **G** Total OHC loss in the middle turn. **F** At the apical end of the apical coil, only a few scattered OHC remain, and there is ongoing damage to OHC. *Scale bars*, 10 μm (**A–E**, **G**, and **H**) and 20 μm (**F**).

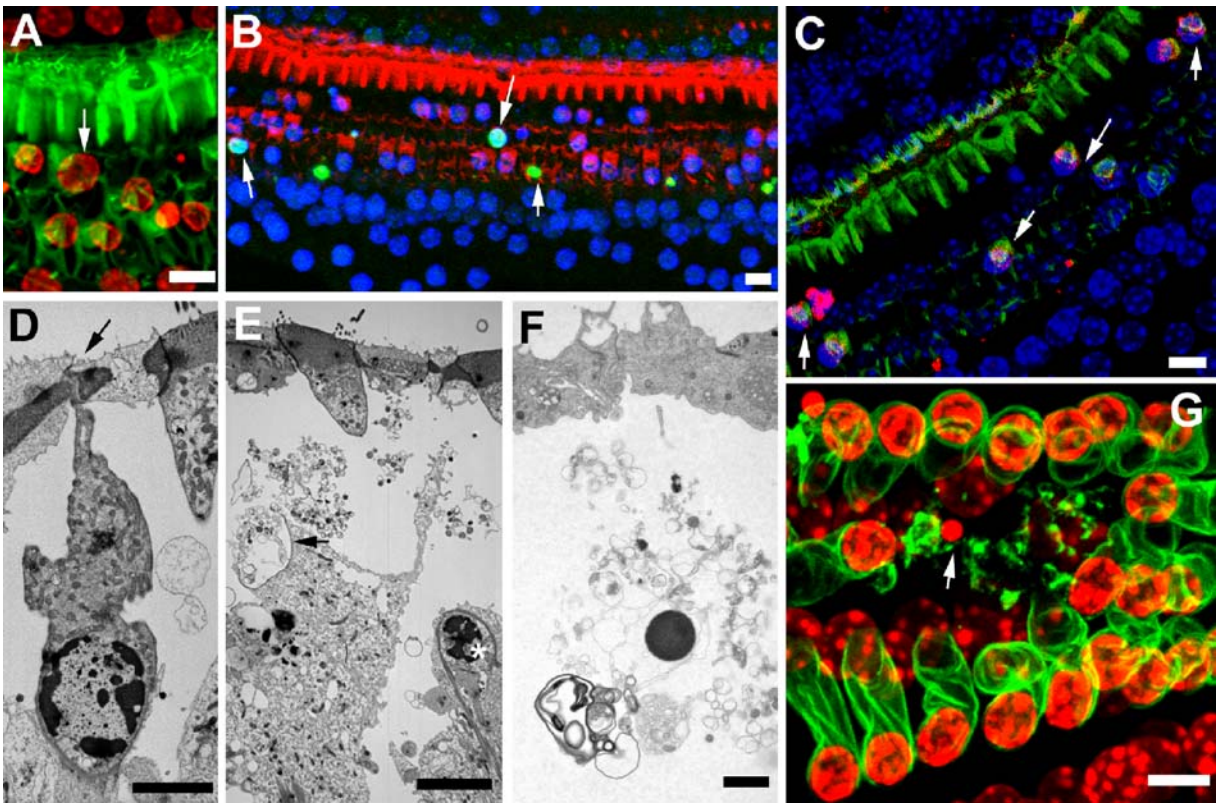

FIG. 2. OHC death. **A** Transitional zone at 24 h posttreatment. Confocal image of whole mount preparation labeled for actin (*green*), with nuclei labeled with propidium iodide (*red*). A single enlarged nucleus, suggesting necrosis (*arrow*), in an OHC (hair bundle labeled with phalloidin), amongst OHC nuclei with apoptotic features. *Scale bar,* 10 μm. **B** TUNEL in region of ongoing hair cell death at 24 h posttreatment. Confocal image of whole mount preparation. TUNEL (*green*), actin (*red*), DAPI (*blue*). Several nuclei (*arrow*) are TUNEL-positive, and all of those are also condensed. *Scale bar,* 10 μm. **C** Activated caspase-3 labeling at 24 h posttreatment. Activated caspase-3, *red*; actin, *green*; DAPI, *blue*. *Arrows* indicate caspase-3-positive hair cells with nuclei that display apoptotic characteristics. Some of these cells also have intact hair bundles. *Scale bar* 10 μm. **D** OHC in thin section through region of ongoing OHC death at 24 h posttreatment. Cell shape is distorted, (compare with adjacent intact cell) and nuclear chromatin is marginated. The apical end of the cell appears to have been lost, suggesting fragmentation of the cell; at the *arrow,* there is a depression where repair of the lesion by expansion of the supporting cells has taken place. *Scale bar,* 5 μm. **E** Thin section through region of ongoing hair cell loss. Condensed chromatin in nucleus of OHC at the *asterisk*. Cellular debris within the extracellular spaces of the organ of Corti. Debris fills the Deiters' cell cup that normally encloses the base of the OHC (*arrow*), suggesting debris derives from ruptured OHC. *Scale bar,* 10 μm. **F** Membranous cellular debris surrounding electron-dense structure resembling an apoptotic nucleus at the level expected of an OHC nucleus at 24 h posttreatment. *Scale bar,* 2 μm. **G** Labeling for prestin (*green*) and nuclei (DAPI shown in *red* for clarity) in region of ongoing OHC loss at 24 h posttreatment. Prestin-labeled fragments surround condensed, apoptotic-like nuclear material (*arrow*). Adjacent to this, other irregular material labeled for prestin is present in spaces from which intact OHC bodies are missing. Elsewhere, prestin labeling delineates the shape of the bodies of OHC. Other apoptotic nuclei are also evident. *Scale bar* 10 μm.

of fluid from the injection site, and in others the injected bolus persisted for some time under the skin. It is likely that these animals received a lower systemic dose or there was slow uptake of the drug and this may account for the absence of damage in a proportion of injected animals. However, the animals in which this potentially inadequate dosing occurred were not systematically recorded, particularly in the earlier stages of the study, so whether the animals in which this happened were the only ones to show no effect after treatment is uncertain.

There was no obvious effect on the vestibular system. There was no evidence of hair loss in either utricular maculae or cristae, and no abnormal behavior was observed in any of the experimental mice in which loss of cochlear hair cells had occurred.

Effects on the organ of Corti

Pattern and extent of OHC loss. No damage, neither hair cell loss nor nuclear abnormalities, was detectable in phalloidin and DAPI-stained whole mounts from cochlea obtained at 6 h postinjection. At 18 h posttreatment, there was OHC loss in the basal coil. By 24 h, loss of all OHC in approximately the entire basal half of the cochlea was evident, and by 48 h, OHC loss had spread to the apical coil (Fig. 1). At 24 h posttreatment,

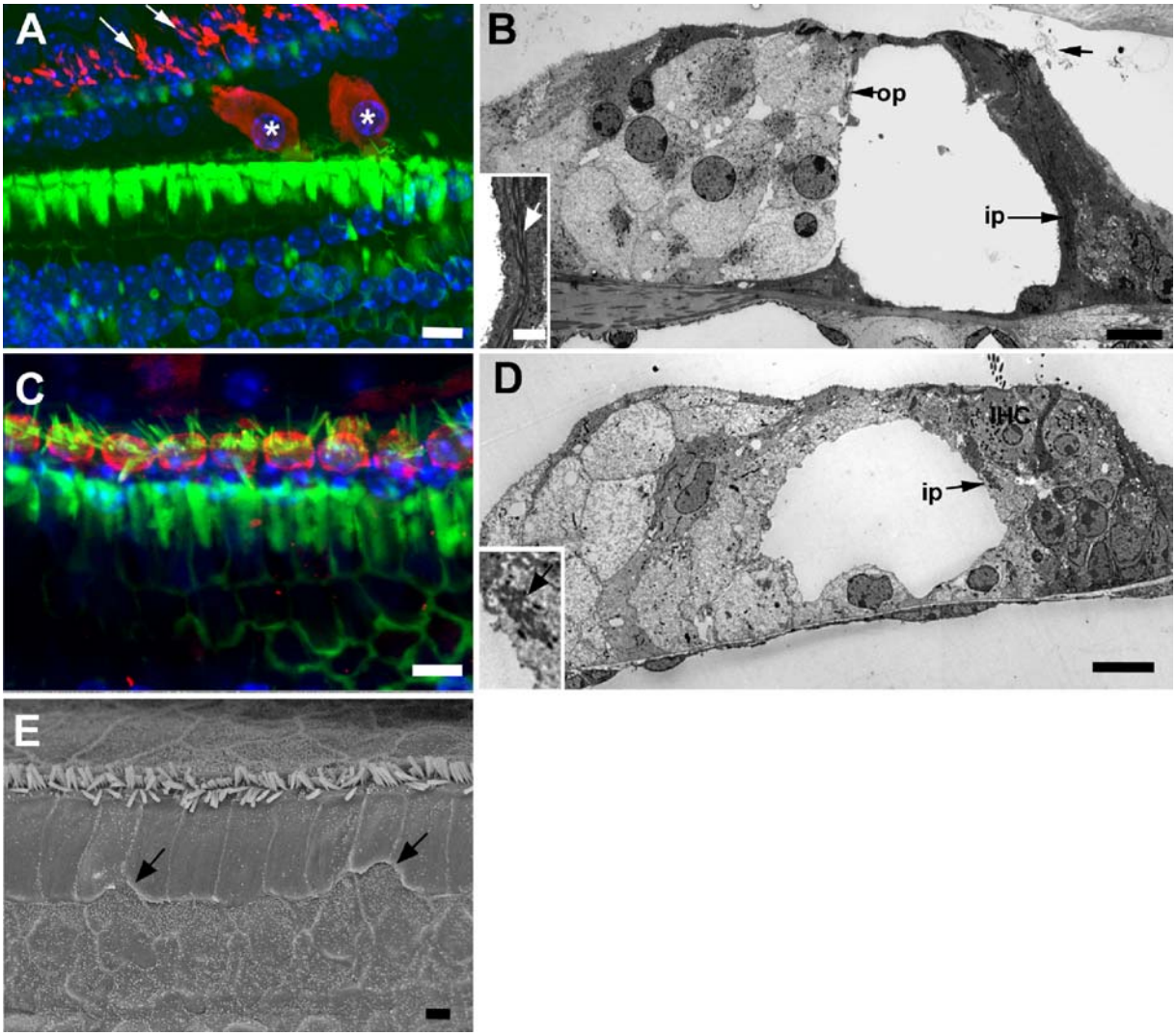

FIG. 3. Progression of damage in the organ of Corti 7 days to 3 months. **A** Seven days posttreatment. Confocal image of whole mount preparation (projection of sections through 18-μm depth of tissue) labeled for calretinin (*red*), with phalloidin-FITC (*green*) and with DAPI (*blue*). Most IHC are lost, but two remain intact (*asterisks*). Afferent nerves (*arrows*) also remain. *Scale bar,* 10 μm. **B** Fourteen days posttreatment. Thin section of upper basal coil. IHC and all OHC are missing. Cell debris (*arrow*) in the endolymphatic space above the normal location of the IHC suggests IHC loss is ongoing at this time. Expanded Deiters' cells fill the space in the OHC region. The arch of Corti is maintained; phalangeal processes of outer pillar (*op*) (cut at an angle) and inner pillar (*ip*) cells retain microtubule bundles shown in the *inset* at higher power, in which the *arrow* indicates the microtubule bundle. *Scale bar,* 10 μm; *inset* 2 μm. **C** Eight weeks posttreatment. Confocal image of whole mount preparation (projection of sections through 18-μm depth of tissue); calretinin (*red*), phalloidin-FITC (*green*), DAPI (*blue*). The presence of the hair bundles and the calretinin-positive cell bodies show that all IHC persist, when all OHC have been lost. *Scale bar,* 10 μm. **D** Twelve weeks posttreatment. Thin section of basal coil. IHC are still present. The arch of Corti is maintained and the microtubule bundles of inner pillar cells (*ip*) are evident, shown at higher power in the *inset*, the *arrow* indicating the microtubule bundle. *Scale bar,* 10 μm. **E** Six weeks posttreatment. SEM of middle coil. All IHC are still present. OHC replaced by expansion of heads of the supporting cells. *Arrows* indicate sites of partial retraction of the head of the inner pillar cell to expose the head of the outer pillar cell at the apical surface. *Scale bar,* 1 μm.

regions of OHC loss were separated from regions of no loss by a "transitional zone," where scattered hair bundles existed amongst scars formed by the apical expansion of neighboring supporting cells to close the lesions resulting from OHC loss (Fig. 1B). Basal to this zone, there was total OHC loss (Fig. 1A), and apical to it, apparently intact OHC were present in all rows (Fig. 1C). By 48 h, the zone of ongoing death of OHC was confined to the apical end of the apical turn (Fig. 1F,H) with total OHC loss basally (Fig. 1D,E,G); often at this time, few OHC remained except at the extreme apex. At this stage, labeling with antibody to the calcium-binding protein calretinin, a preferential label of inner hair cells (IHC) and neurons (Fig. 1D), as well as SEM (Fig. 1G,H), revealed that all IHC were still present.

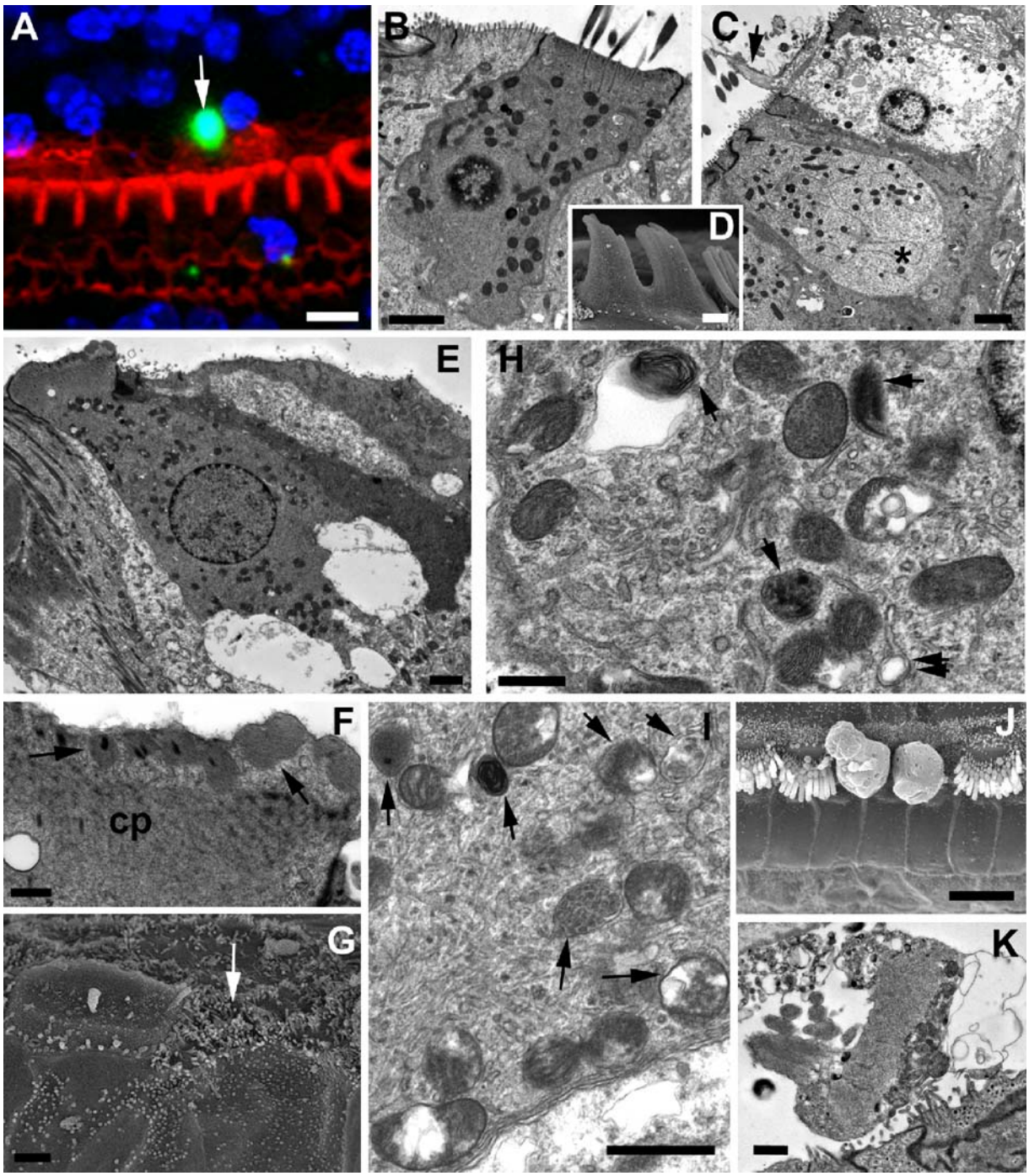

OHC death

The presence of a "transitional" zone between regions of complete OHC loss and no loss afforded the opportunity to examine the region of ongoing hair cell death. Within this region, the majority of remaining OHC nuclei appeared apoptotic, with marginated and condensed chromatin as demonstrated with either propidium iodide or DAPI (Fig. 1A–C). Infrequently, a swollen nucleus was apparent amongst the apoptotic nuclei, suggesting that, in some instances, cells died via a necrotic pathway (Fig. 2A).

Apoptotic cells can be detected by terminal deoxynucleotidyl transferase (TdT)-mediated 2′-deoxyuridine 5′-triphosphate nick end labeling (TUNEL) in which the free 3′-OH termini of fragmented DNA are labeled with modified nucleotides. TUNEL-positive nuclei were located in the region of OHC loss at both 24 h posttreatment and 48 h (Fig. 2B). In all TUNEL-positive cells, the nuclei were pyknotic, with condensed chromatin. There were no TUNEL-positive nuclei in undamaged control tissue (not shown). To clarify whether hair cells died via a classical apoptotic

◀**FIG. 4.** IHC loss. **A** TUNEL in whole mount preparation at 7 days posttreatment. TUNEL, *green*; actin, *red*; nuclei with DAPI, *blue*. In a region of scattered IHC loss, one IHC nucleus is TUNEL-positive. *Scale bar*, 10 μm. **B** Thin section 4 weeks posttreatment. IHC with features of apoptosis: condensed cytoplasm and distorted shape (compare cytoplasmic density and contour with normal IHC cut in the same plane in **C** indicated with an *asterisk*), and the nucleus shows condensed, marginated chromatin. The stereocilia appear largely intact. *Scale bar*, 2 μm. **C** IHC (4 weeks posttreatment) showing evidence of necrosis; loss of cytoplasmic contents. The stereocilia are fused (*arrow*). Adjacent IHC has normal appearance. *Scale bar*, 2 μm. **D** SEM of extensively fused stereocilia on an IHC (7 days posttreatment) similar to those in section in **C**. *Scale bar* 1 μm. **E** IHC 4 weeks posttreatment. The cytoplasm is condensed (compare high density with lower cytoplasmic density of normal IHC labeled in **C**, indicated with an *asterisk*), but the nucleus and cell shape are normal. Sites of afferent nerve endings at the base of the cell are swollen. At the apex, the stereocilia are withdrawn into the cell body and the cuticular plate is separated from the apical membrane. This apical region is shown at higher power in **F**. *Scale bar*, 2 μm. **F** Apex of the IHC in **E**. The stereocilia (*arrows*), some with the rootlets evident, are withdrawn beneath the apical plasma membrane and a strip of cytoplasm separates the apical plasma membrane from the leading edge of the cuticular plate (*cp*) in which stereociliary rootlets are also apparent. *Scale bar*, 0.5 μm. **G** SEM of region of ongoing IHC death. The apical surface of one IHC (to the *left*) has only a vestigial stereocilium, and the apical surface is smooth with no impressions of broken stereocilia, indicating that the loss stereocilia is not due to preparation damage. The site from which the adjacent IHC has been lost (*arrow*) is closed by expansion of the surfaces of inner phalangeal and inner border cells. *Scale bar*, 1 μm. **H**, **I** Cytoplasmic vesicles in two different IHC with condensed cytoplasm. Panel H is a region of the cell shown in **E**. *Arrows* indicate membrane-bound vesicles enclosing cellular debris. Multivesicular bodies and multilamellar vesicles can be identified. *Double arrow* in **H** indicates forming double-membraned vesicle. *Scale bars*, 0.5 μm. **J** SEM, **K** thin section of apical fragment of IHC at the surface of the organ of Corti in region of ongoing IHC loss. In section, the fragment is seen to contain some apparently intact mitochondria, the cuticular plate and the stereocilia. *Scale bars*, 10 μm (**J**), 1 μm (**K**).

pathway, immunohistochemistry was performed using an antibody to detect activated caspase-3, an effector of the caspase-dependent apoptotic pathway. This revealed cells positive for activated caspase-3 within the transitional zone (Fig. 2C). The nuclei of these cells were typical of apoptotic cells: pyknotic, with marginated or condensed chromatin. Phalloidin labeling revealed that hair bundles were retained on a number of cells positive for activated caspase-3, demonstrating that the hair cell death can already be underway prior to any obvious damage to stereocilia. No labeling for activated caspase-3 was found in areas of complete OHC loss, nor in undamaged control tissue (not shown).

In TEM of thin sections, regions of ongoing OHC death could be identified in the middle turn of the cochlea at 24 h and in the apical turn at 48 h posttreatment. In such regions, many OHC displayed morphological characteristics of apoptosis: nuclei with marginated and condensed chromatin, condensed cell cytoplasm, and distorted cell shape (Fig. 2D,E). OHC showing the morphological features of necrosis were not found in thin sections, but scattered debris apparently from ruptured OHC was free within the extracellular spaces of the organ of Corti at the locations of missing OHC (Fig. 2E,F). Often, such debris enclosed what appeared to be condensed chromatin – similar to an apoptotic nucleus – (Fig. 2F) at levels in the epithelium expected of an OHC nucleus. Confocal light microscopy of whole mount samples immunohistochemically labeled for prestin confirmed that such debris was derived from OHC. Within the spaces of the organ of Corti, irregular material, positively labeled for prestin, surrounded dense DAPI-labeled bodies indicative of condensed nuclear chromatin at the position of OHC nuclei (Fig. 2G). In the regions of the organ of Corti just basal to the area of ongoing hair cell degeneration where hair cell loss was complete, there was no debris, suggesting such cell fragments were cleared rapidly.

IHC death and survival

Total loss of OHC preceded any IHC loss, which was always significantly delayed in relation to loss of OHC, but it was inconsistent as to timing postinjection and variable in its occurrence. With the exception of the cochleae of one animal taken at 4 days postinjection, no IHC loss was apparent until at least 7 days posttreatment, and it was most frequently observed in samples taken at 2 and 4 weeks posttreatment. At both these times, whereas in some cochleae IHC loss appeared to be almost total along the entire length of the organ of Corti, in others it appeared to be ongoing, suggesting relatively recent initiation (Fig. 3A,B). In these latter examples, IHC loss could be seen generally to proceed base to apex, but sometimes, there was scattered loss of IHC, individual or groups of apparently intact IHC persisting within regions of otherwise absent IHC (Fig. 3A). However, loss of IHC did not always occur in cochleae in which there was total loss of OHC. In more than half of the cochleae from treated mice taken at 7 days posttreatment and later (32 out of 59) in which all OHC along the entire length of the organ of Corti had been lost, IHC persisted (Fig. 2C,D). Even in some animals taken at 3 months following injection in which there was total OHC lost, all IHC remained.

As described above, IHC death was considerably delayed in comparison with OHC death, and in more than half the cochleae examined from 2 weeks onwards in which all OHC were lost, IHC were still present. In regions of ongoing IHC loss, some nuclei were TUNEL-positive (Fig. 4A), suggesting apoptotic cell death. Thin sections through regions of ongoing IHC death revealed a variety of features associated with degener-

ation in different cells. In many IHC, nuclear chromatin was condensed and marginated, the cell cytoplasm was condensed and cell shape distorted, although mitochondria appeared largely normal (Fig. 4B). These cells with morphology consistent with apoptosis often possessed seemingly intact hair bundles. A few IHC displayed ruptured plasma membrane and loss of cytoplasmic contents, features consistent with necrosis (Fig. 4C). In such cells, stereocilia were often fused, and extensively fused stereocilia upon IHC were evident in SEM (Fig. 4D). Other IHC, whose shape and nuclei appeared normal, had an unusually electron dense cytoplasm, suggesting condensation of cytoplasmic contents, but there were also swellings around the base of the IHC at the sites of the afferent nerve terminals (Fig. 4E). Many IHC with this morphology seemed to be resorbing their stereocilia; the microfilament bundles were enclosed beneath the apical plasma membrane (Fig. 4F). In SEM, IHC with no or only vestigial stereocilia were apparent amongst hair cells with normal hair bundles and close to the sites of missing IHC (Fig. 4G). The apical surface of the membrane of these cells appeared smooth, with no indications of the sites of the stereocilia. The apical cytoplasm of cells with internalized stereocilia contained numerous vesicles, often double-membraned, enclosing cellular material (Fig. 4H,I). These structures are reminiscent of autophagic vesicles in various stages of the autophagic progression (Eskelinen 2005).

At least some IHC appeared to fragment just below the level of the cuticular plate with the apical fragment released into the endolymphatic space. SEM revealed globular structures, reminiscent of cellular material, at the apical surface at the sites of IHC (Fig. 4J). Apical fragments of IHC, consisting of stereocilia, the cuticular plate, and some cytoplasmic material containing apparently intact mitochondria, were sometimes found lying atop the reticular lamina above the locations of IHC, in the endolymphatic space below the tectorial membrane (Fig. 4K).

FM1-43 labeling of hair cells

One reason for the persistence of IHC when OHC die might be that they do not take up aminoglycoside as readily as OHC. To examine this issue, we investigated the uptake of the fluorescent lipophilic dye FM1-43 into hair cells in the mature organ of Corti. FM1-43 is of similar size to aminoglycoside (MW FM1-43 452, kanamycin 484) and, like aminoglycosides, FM1-43 is a cation. In sensory epithelia of the inner ear, FM1-43 preferentially labels hair cells. It has been suggested that the dye enters hair cells via the transduction channel at the tip of the stereocilia (Gale et al. 2001; Meyers et al. 2003), and because aminoglycosides can bind to the transduction channel and FM1-43 can inhibit the aminoglycoside-induced injury to hair cells in organotypic culture of the early postnatal organ of Corti, it has been argued that FM1-43 and aminoglycosides enter hair cells by the same route (Gale et al. 2001). Consequently, FM1-43 may act as a nontoxic "mimic" for aminoglycosides.

When the isolated, intact, but opened, mature cochleae were exposed to FM1-43 for 10 s, dye labeling was present in both IHC and OHC (Fig. 5A). Labeling in IHC was at least as intense if not greater than that in OHC. This suggested that the dye may be able to enter IHC and OHC equally readily in the mature cochlea.

However, it is possible that the isolation of the cochlea, opening it, and the exposure to in vitro conditions lead to abnormal, sustained opening of the transduction channels in both OHC and IHC and/or the dye is not efficiently washed away and uptake occurs through several routes, including endocyototic activity (although the use of low temperatures for postexposure washing in buffer maintained on ice was included to restrict endocytotic activity). Thus, the entry of FM1-43 into hair cells in vivo and the effects of coadministration of bumetanide upon uptake were examined. Two hours after administration either with or without coadministration of bumetanide, no dye uptake was evident in the organ of Corti. At 6 h after systemic injection of FM1-43 in conjunction with bumetanide, both IHC and OHC in the lower apical coil were labeled (Fig. 5B). At 24 h, IHC and OHC were both labeled, IHC seemingly more intensely than OHC (Fig. 5C). In the cochleae of mice that received only FM1-43, but not bumetanide, there was very little labeling of the hair cells at 6 h, and the intensity of labeling at 24 h (Fig. 5D) appeared less than in the cochleae of animals coadministered the diuretic, but again, both IHC and OHC were labeled. In utricular maculae from mice coadministered FM1-43 and bumetanide, the intensity of FM1-43 labeling in hair cells was markedly lower than that in organs of Corti of the same set of animals (Fig. 5E) and very little different from labeling of utricular hair cells in mice that received only FM1-43. However, dye labeling was present and quite intense in the capillaries underlying the utricular macula, demonstrating that FM1-43 had reached the vestibular organs (Fig. 5E).

Supporting cell rearrangement following OHC loss

The loss of OHC was accompanied by closure of the lesions by expansion of supporting cells into the area once occupied by the hair cell. Neither in SEM preparations (Fig. 6A,B) nor in thin sections (Fig. 6C) was there evidence of obvious lesions breaching through the reticular lamina as hair cells died, suggesting that, despite the rapid and extensive loss of OHC, lesion repair still occurred efficiently and in a manner similar

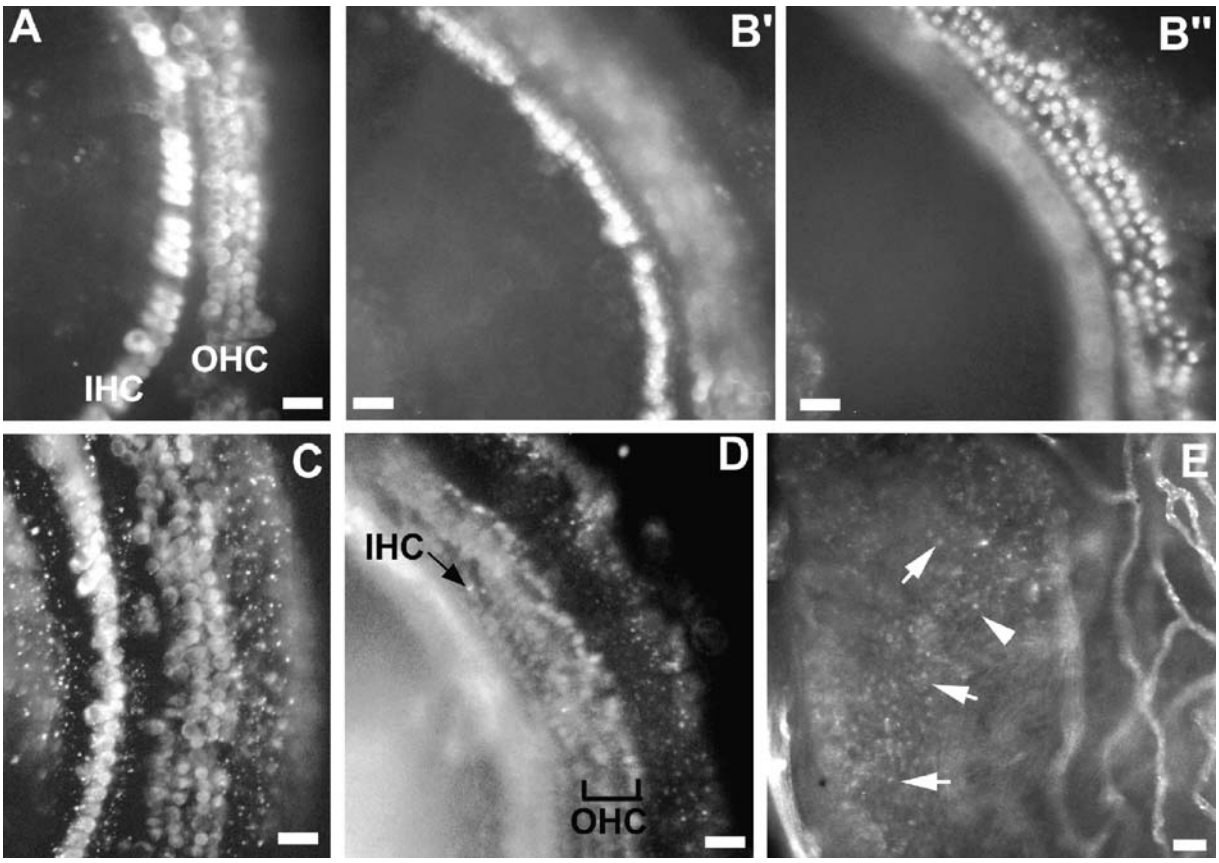

FIG. 5. FM1-43 uptake. **A** In vitro isolated cochlea exposed for 10 s at 37°C; lower apical cochlear coil. FM1-43 has labeled only hair cells and has labeled both IHC and OHC. **B** Organ of Corti 6 h after coadministration of FM1-43 and bumetanide in vivo. Middle coil. Same sample shown in **B′** as **B″** with focus at level of IHC in **B′** and OHC at **B″**. FM1-43 is present in both IHC and OHC. **C** Twenty-four hours after coadministration of FM1-43 and bumetanide in vivo. Middle turn. Again both IHC and OHC are labeled. **D** Twenty-four hours after injection of FM1-43 only in vivo. FM1-43 is present in both IHC and OHC, but the intensity of labeling is less than when the bumetanide is coadministered with the dye. **E** Utricular macula 24 h after coadministration of FM1-43 and bumetanide. Hair cells (*arrowed*) are labeled but not as intensely as cochlear hair cells in similar samples. Capillaries (to the *right*) show quite intense FM1-43 label. *Scale bar,* 20 μm (**A**–**D**), 50 μm (**E**).

to that described previously for OHC loss following chronic gentamicin treatment in guinea pigs (Forge 1985). At the apical surface of the reticular lamina at the site from which an OHC was missing, there was a depression, the shape of a hair cell apex, that was closed at its base, indicating supporting cells had already closed the lesion (Fig. 6A). Other stages in ongoing repair captured at the time of tissue fixation also revealed the closure of the lesion as hair cell remnants separated, and the absence of open wounds (Fig. 6B). In thin sections (Fig. 6C), the site at the reticular lamina of a missing hair cell was identifiable by a depression in the surface, sometimes with some cellular debris within it, and immediately below it, the lesion was closed by a junction between adjacent supporting cells with the electron density of a tight junction, indicating the sealing of the lesion as the hair cell died.

There was considerable structural reorganization amongst the supporting cells during and following lesion closure. Normally, the phalangeal processes of Deiters' cells rise at an angle from the cell body region, enclosing one OHC body to contact the apices of OHC at least one OHC distant crossing over another OHC body on the way (Fig. 6D). In the repaired organ of Corti, the Deiters' cell phalangeal processes rose straight up from the cell body without angulation, suggesting movements of the heads of the supporting cells at the level of the reticular lamina (Fig. 6E,F). Some Deiters' cells were rounded as the reorganization proceeded and the cell body enclosing the nucleus was at a more apical (luminal) position than normal (Fig. 6F,G); although, whether these cells lost contact with the basilar membrane was not confirmed. Despite these morphological changes, Deiters' cell bodies retained close contact with their neighbors (Fig. 6G). The repaired epithelium was narrower, with the outermost edge of the epithelium closer to the pillar cells than in undamaged tissue. The epithelial surface was buckled so that an inward furrow was created along the length of the epithelial surface with the Hensen's closely approaching the pillar cells (Fig. 6H,I). However,

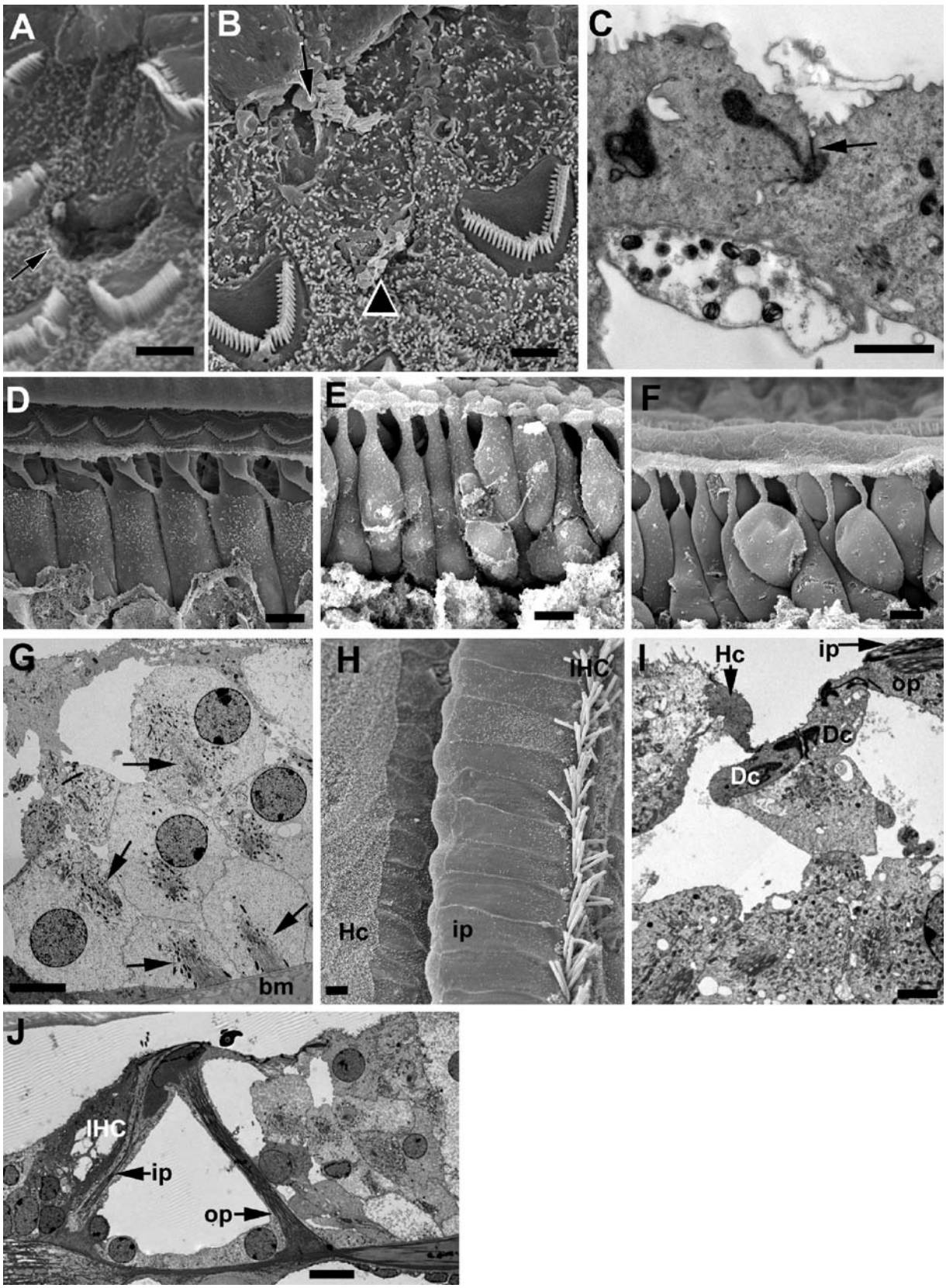
A
B
C
D
E
F
G
bm
H
IHC
Hc
ip
I
Hc
ip
op
Dc
Dc
J
IHC
ip
op

FIG. 6. Supporting cell reorganization. **A** In a region of ongoing OHC loss, a depression in the reticular lamina at the site of a lost hair cell (*arrow*) is closed at the bottom. *Scale bar,* 5 μm. **B** Apical fragments of OHC are being lost from the surface (*arrow* and *arrowhead*) to reveal the closed lesion beneath. Stereocilia of the released OHC apical fragment are evident at the *arrow*. *Scale bar,* 5 μm. **C** Thin section through the reticular lamina in the region of ongoing hair cell loss. Cellular debris at the surface of the reticular lamina lies within a depression where two supporting cells meet. Cell debris is also present in the space below the supporting cells. At the *arrow,* the junction between the supporting cells shows the electron density characteristic of a tight junction, suggesting sealing of the lesion site as OHC fragment. *Scale bar,* 1 μm. **D** Normal, intact organ of Corti. SEM view of the third (outermost) row of Deiters' cells in the basal coil. The cell bodies of Deiters' cell, covered with microvilli, enclose smooth-surfaced OHC. The phalangeal processes of each Deiters' cell rises at an angle from the cell body to the reticular lamina to contact the OHC at least one away from that which its own body encloses. *Scale bar,* 10 μm. **E** SEM, 2 days posttreatment. Upper basal coil. All OHC have been lost. The phalangeal processes of Deiters' cells are straight. *Scale bar,* 10 μm. **F** SEM, 7 days posttreatment. The cell bodies of some Deiters' cells in the third and second row have rounded up. *Scale bar,* 10 μm. **G** Thin section through Deiters' cell region, 14 days posttreatment. The cell bodies of many Deiters' cell are rounded and the nuclei of some of them are located at a more apical level than that found in normal tissue. Microtubules bundles (*arrowed*) are at the cell base at the site of contact with the basilar membrane (*bm*), as well as at higher levels in the cell body. *Scale bar,* 5 μm. **H** SEM, 14 weeks posttreatment. Apical surface of the reticular lamina. All OHC are lost. Hensen's cells (*Hc*) approach inner pillar cells (*ip*). The surfaces of the Deiters' appear to be disappearing into the fold created at the surface becoming covered by the head of the inner pillar. All IHC appear to be surviving. *Scale bar*: 1 μm. **I** Furrow at apical surface of organ of Corti after hair cell loss. Thin section. Four weeks posttreatment. Hensen's cells approach inner pillar (*ip*), with Deiters' cells (*Dc*) at the bottom of the fold. The head of the inner pillar cell has retracted so that the head of the outer pillar cell (*op*) is exposed at the apical surface. *Scale bar,* 2 μm. **J** Two weeks posttreatment. Thin section through organ of Corti. All OHC missing and there is considerable reorganization in the Deiters' cell region. IHC is degenerating. The arch of Corti is erect and supported by inner pillar (*ip*), and outer pillar (*op*) cells, which show no obvious loss of specializations; the microtubule bundles within both pillar cell types are intact. *Scale bar*: 10 μm.

although there was rearrangement of Deiters' cells, they retained most of their obvious structural specializations, including prominent, organized microtubule bundles in the cell body region and at the base of the cell in contact with the basilar membrane (Fig. 6G). Other than the expansion of the head of the outer pillar cell to close lesions where OHC in the first row were lost (Fig. 6A,B), and retraction of the head of some inner pillar cells (Figs. 3C and 6I), there was little alteration of the phalangeal processes or cell bodies of the pillar cells. The tunnel of Corti remained widely open (Fig. 3B,D), flanked by the phalangeal processes both of the outer and the inner pillar cells, which remained erect, supported by their bundles of microtubules, which remained undisturbed (Fig. 6J). Overall, there was little structural evidence of any significant de- or redifferentiation of supporting cells even after quite prolonged periods following loss of OHC.

Despite considerable reorganization of the sensory epithelium in the OHC region, in many cases, IHC persisted (Figs. 3C and 6H). They remained even when there was buckling of the reticular lamina caused by the inward movement of the Hensen's cells (Fig. 6H). Conversely, there was IHC loss when pillar cells and the arch of Corti were intact (Figs. 3B and 6J). The death of IHC, when it occurred, therefore, did not appear to be directly related to the reorganization of the epithelium occasioned by death of OHC and the subsequent structural rearrangements amongst the supporting cells.

Effects on the SV

In TEM sections from control animals (Fig. 7A), and from those which had received the drugs but showed no effect upon the hair cells ("undamaged, injected" animals), no obvious abnormalities of the stria were detected. Administration of a single dose of bumetanide is known to cause extensive edema in the stria by 1 h following injection, but this rapidly resolves and no continuing abnormalities are evident by 24 h posttreatment (Santi and Duvall 1979). There was no edema in the SV of any animal taken at 24 h posttreatment in which there was hair cell loss (Fig. 7B), and in these mice, the stria appeared no different from that of controls or undamaged, injected animals. Likewise, there were no obvious abnormalities in the striae of any animal taken at 2–4 days posttreatment in which there was hair cell loss. Measurements of the thickness of the striae in these animals (basal coil; mean 35.01 μm, range 24.6–45.8 μm; apical coil: mean 29.6 μm; range 21.1–37.0 μm) showed no significant difference from that of controls (basal coil: mean 34.1 μm, range 28–42 μm; apical coil: mean 31.1 μm; range 28.7–34.8 μm) (Fig. 8). Striae of two untreated older mice, one aged 12 months the other 2 years old, were also examined. There was no detectable hair cell loss at 12 months, and at 2 years, there was a very low level of scattered hair cell loss, and the mean strial width in these animals (12 months, 32.2 μm; 2 years, 31.3 μm) was within the normal range (Fig. 7C). There were, however, indications of cellular degeneration in the stria from the 2-year-old animal (Fig. 7C), most noticeably the presence of cells within the body of the stria containing clusters of electron dense inclusions and vesicles filled with amorphous electron dense material.

In contrast, in animals in which there was hair cell loss taken at 7 days posttreatment and at subsequent time points, there was a significant decrease in strial thickness (Figs. 7D,E; 8). One-way ANOVA statistics revealed a significant decrease for both apical and

basal coils at 2 weeks posttreatment in comparison with controls and a further significant decrease between 4 weeks posttreatment and 8 weeks and later times. This would indicate a progressive reduction in strial thickness continuing for some time concomitant with the reorganization of the sensory epithelium following hair cell loss. In some animals at the later time points, (2–3 months) the strial thickness was only 10–12 μm and the basal cell layer was still intact, intermediate cells were difficult to distinguish, and marginal cells were severely reduced (Fig. 7E).

The major cause of the strial thinning appeared predominantly to be a reduction in the basal infoldings of marginal cells (Fig. 7F,G), first apparent in samples taken at 7 days posttreatment, and degeneration of marginal cells themselves (Fig. 9A–G), which was more pronounced in samples taken at 14 days postinjection and subsequently. In damaged cochlea, the extensive basal infoldings were absent from many marginal cells (Fig. 7F) or reduced to thin, apposing stacks of short processes (Fig. 7G), and the interdigitations with intermediate cells were retracted such that ramifying, thin processes of the intermediate cells were revealed (Fig. 7F). What were presumably marginal cells, judging from their location at the endolymphatic surface but which possessed no obvious basal infoldings and were almost cuboidal or rounded in shape, exhibited a reduced electron density in comparison with more normal neighboring marginal cells (Fig. 9A,B). Some cells with this feature (Fig. 9A) were filled with long, almost parallel, closely packed filamentous structures, ca. 20–25 nm in width, reminiscent of microtubules (Fig. 9C,D). These ran throughout the cell, from the apical cell body region (Fig. 9C) to the basal extremities (Fig. 9D). Transverse sections (Fig. 9D) confirmed the microtubule-like character of these structures. At their apical surfaces, some cells exhibited unusual numbers of small microvilli and cell width along the apical plasma appeared reduced concomitant with apparent enchroachment of lateral expansions of the immediately neighboring marginal cells (Fig. 9A,B), such that the affected cell seemed to be becoming enclosed apically and withdrawing into the epithelium. Enclosed within the body of the stria, there were also degenerating cells (Fig. 9E), which the size of their still intact mitochondria suggested were marginal cells. Nuclei in some marginal cells with abnormal features were fragmented with condensed chromatin (Fig. 9A, E) suggestive of apoptosis. Within the stria at a level similar to that of intermediate cells, there were often approximately rounded cells with normal appearing nuclei that contained electron dense inclusions and filled membrane-bound vesicles (Fig. 9F,G), precisely similar to the features indicating cellular degeneration in the stria of the aged 2-year-old mouse (Fig. 7C). Also found in the body of the stria were concentric whorls of membrane enclosing what appeared to be degenerating cellular material (Fig. 9H,I). These latter abnormalities – cells with inclusions and concentric membrane whorls – while occasionally present at 7 days posttreatment, were common in SV at the later time points.

Amikacin or gentamicin with bumetanide

Mice tolerated amikacin as equally well as kanamycin. All animals survived injections with doses of amikacin at 1 mg/g (n=6). When amikacin was administered with bumetanide, complete loss of OHC was evident, but IHC survived for at least 14 days (n=3). As others have noted (Wu et al. 2001), gentamicin was not well tolerated. Single injections of doses greater than 0.3 mg/g caused rapid death of the animals (n=6). Gentamicin at 0.25 mg/g, when given in combination with bumetanide, had no damaging effect on the cochlea (n=3). However, some animals survived injection of gentamicin at 0.3 mg/g followed by bumetanide. In these animals, complete loss of all OHC but persistence of IHC was also evident at 7 (n=3) and 14 days posttreatment (n=2). These observations indicate that the relative resistance of IHC following kanamycin–bumetanide treatment is not drug-specific.

Age effects on OHC loss

In animals at 18–21 days of age, the organ of Corti is structurally mature and the animals can hear. Animals of this age were used partly to keep injection volumes as small as possible, partly because it has been suggested that animals of this age are more sensitive to the aminoglycoside–diuretic combination than older animals (Prieve and Yanz 1984). To test the age-dependence of hair cell loss, animals aged 25, 30, and 35 days (n=3 in each case) were treated and their cochleae examined 7 days after treatment. Complete loss of OHC from base to apex was observed in the 25- and 29-day-old animals, but in two out of the three animals at 35 days, OHC remained in the apical coil, although there was still scattered loss in this region too.

DISCUSSION

The kanamycin–bumetanide protocol used here provides a robust method to induce consistently extensive hair cell loss from the mature organ of Corti in mice. The death of OHC occurs rapidly in a defined pattern the same as that found in many other conditions, both of acquired hearing loss and due to genetic defects, over much longer time scales. In spite of the rapid and extensive loss of OHC, supporting cells appear to close the lesions as efficiently as when hair cell death occurs

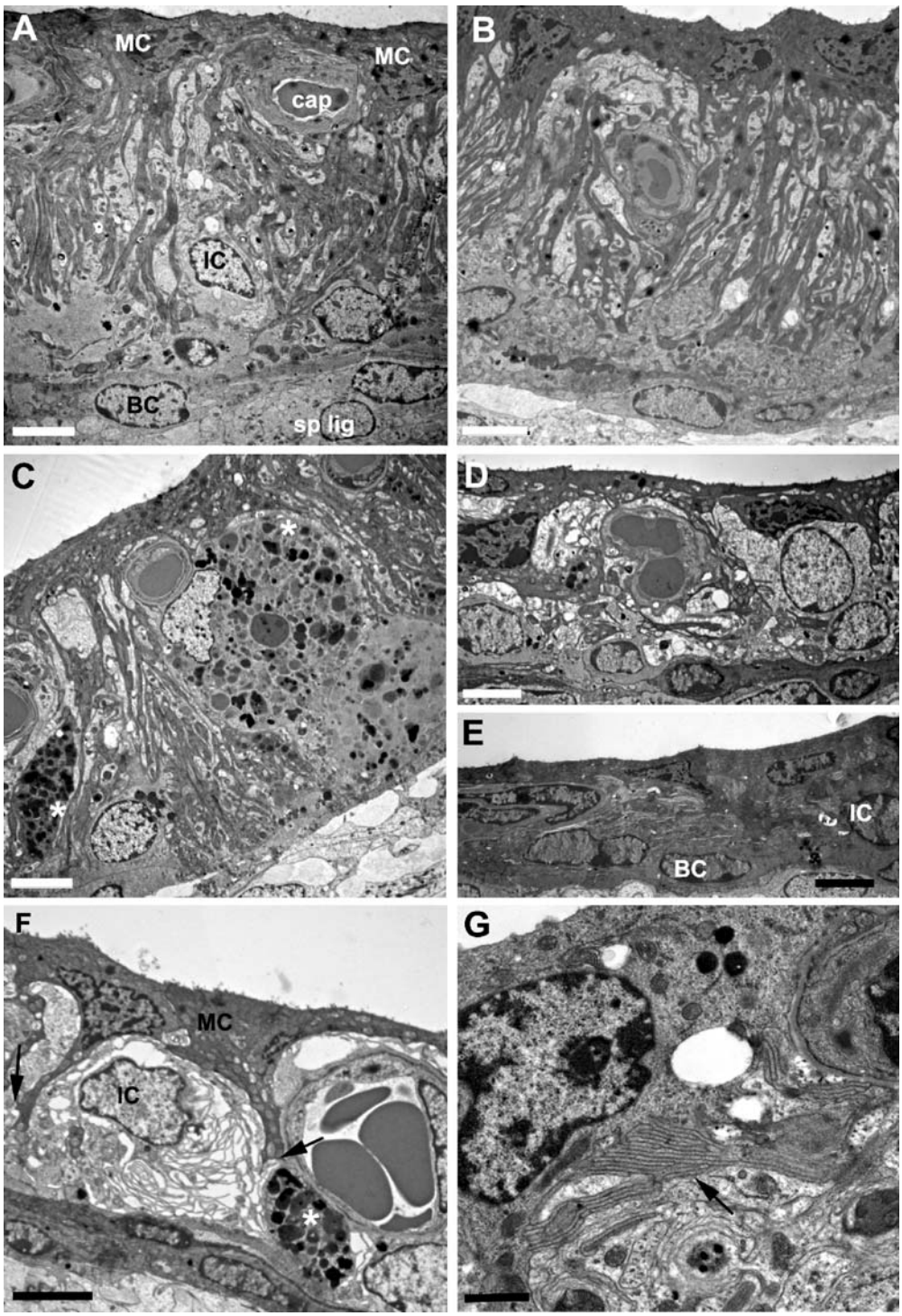

FIG. 7. SV atrophy. **A** Normal SV from an untreated mouse. *MC,* marginal cell; *IC,* intermediate cell; *BC,* basal cell; *cap,* capillary; *sp lig,* spiral ligament. **B** Twenty-four hours after kanamycin–bumetanide treatment. SV looks normal. **C** SV from untreated 2-year-old mouse. Strial thickness (endolymphatic surface to edge of spiral ligament) is within the normal range. Cells (*asterisk*) at level of the intermediate cells contain electron dense inclusions. **D** Two weeks posttreatment; basal turn. There is a significant decrease in strial thickness. **E** Twelve weeks posttreatment; basal turn. Considerable atrophy of the stria has occurred so that the normal architecture is difficult to discern, but basal layer (*BC*) is intact and intermediate cells (*IC*) are recognizable. *Scale bars,* 5 μm (**A**–**E**). **F** In thinning stria in the basal coil at 2 weeks posttreatment, marginal cell (*MC*) basal processes are truncated (*arrows*), whereas intermediate cell (*IC*) processes are exposed by withdrawal of those of the marginal cells. *Asterisk* indicates electron dense inclusions inside cells at level of intermediate cell. *Scale bar,* 5 μm. **G** Clustered stacks of marginal cell processes devoid of mitochondria (*arrow*). *Scale bar,* 1 μm.

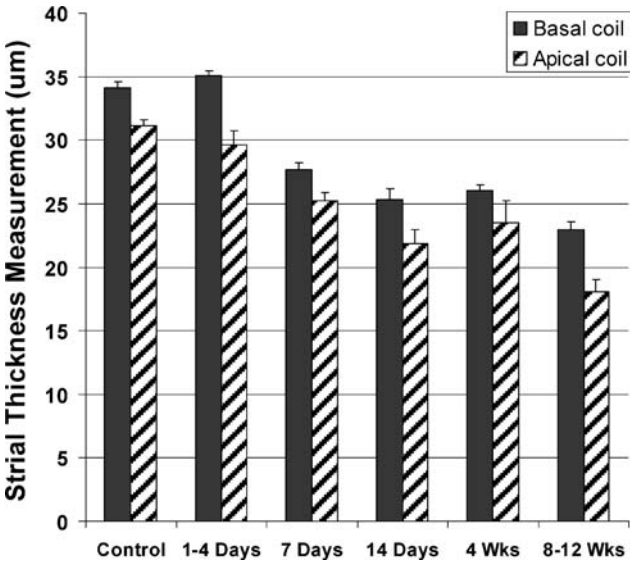

FIG. 8. Mean (±SEM) of strial thickness at different times posttreatment. The thickness of the SV was measured in the basal and apical coils in the same sections. *N* for control=6; 1–4 days=7; 7 days=3; 14 days=12; 4 weeks=3; 8–12 weeks=4. The thickness at all posttreatment time groups 7 days to 8–12 weeks is significantly less than control. The thickness in the 8–12 weeks group is significantly less than in the 4 weeks group ($p<0.001$).

less extensively, and structural reorganization of the supporting cell region of the organ of Corti ensues. In general, the repair process shows features previously reported following chronic hair cell loss regimes in guinea pigs (Forge 1985; Raphael and Altschuler 1991). The reorganization involves considerable movements of the Deiters' and Hensen's cells, as well as changes in cell shape and, in some Deiters' cells, a relocation of the nucleus to a more apical position, though whether any of these cells also lose contact with the underlying extracellular matrix of the basilar membrane could not be confirmed. However, over the time scale examined, supporting cells appeared to retain most of their normal structural specializations with little evidence of any dedifferentiation. Further studies of whether functional specialization of supporting cells is retained following hair cell loss are currently underway. Both in animals and in humans, at prolonged periods following loss of all hair cells, continuing remodeling of the remaining supporting elements of the organ of Corti ultimately results in its replacement by a thin, nonspecialized epithelium covering the basilar membrane. Death of supporting cells may occur during this progression (Ladrech et al. 2007). The movement of the Hensen's cells towards the pillar cells, that was seen in the present work, and which would lead to Deiters' cells becoming covered over lumenally and enclosed within the epithelium, may herald the initiation of these further steps in the epithelial remodeling. However, neither obvious death of supporting cells, nor the complete replacement of the organ of Corti was seen over the period of up to 3 months after treatment that was examined. Studies of the cochleae of mice taken after longer periods following the treatment are currently in progress. Nevertheless, the results presented here suggest that the protocol used does potentially provide a means to examine the mechanisms of hair cell death and the response of supporting cells in the cochleae of mature mice in vivo, which can be applied in transgenic animals to explore the molecular basis of repair and recovery processes.

Loop diuretics such as bumetanide are not thought to act directly on hair cells nor to have any long-term effects in the cochlea, and no such effects of bumetanide on its own were found here. Single doses of kanamycin on their own also caused no obvious damage to the organ of Corti or SV in either the short or long term. However, loop diuretics are known to significantly enhance uptake of aminoglycosides into the endolymphatic compartment of the cochlea (Tran Ba Huy et al. 1981), whereas perilymphatic levels of aminoglycoside are not increased by coadministration of a loop diuretic (Russell et al. 1979). If a major route of aminoglycoside entry to the hair cell is via the transduction channels at the tips of stereocilia (Gale et al. 2001; Marcotti et al. 2005; Waguespack and Ricci 2005), then facilitation of uptake to the endolymph would facilitate access of aminoglycoside to its site of hair cell entry. The results from the studies of FM1-43 support this contention. FM1-43 is similar in size and charge to aminoglycoside. The diuretic significantly enhanced its uptake into cochlear hair cells over that which occurs with administration of dye alone. Although FM1-43 may enter IHC through endocytotic activity at the basal pole (Griesinger et al. 2002), the major site of entry is thought to be through the transduction channels (Gale et al. 2001; Meyers et al. 2003). Thus, the diuretic can facilitate access of the dye to the endolymphatic compartment of the cochlea and the apical poles of the hair cells. Furthermore, while dye entry into cochlear hair cells was enhanced, entry into vestibular hair cells was not, a pattern of dye distribution that mirrors the pattern of hair cell loss. The bumetanide–kanamycin combination produced extensive death of cochlear hair cells, but the vestibular organs were completely unaffected, a differential sensitivity to a diuretic–aminoglycoside combination also found in chinchillas (McFadden et al. 2002). Thus, the dye appears to be a tracer for the distribution of the damaging agent. It seems likely, therefore, that the death of cochlear hair cells following kanamycin–bumetanide treatment is a result of the action of the aminoglycoside upon them, whereas the diuretic acts to promote the very rapid entry of a high concentration of the aminoglycoside into the endolymphatic compartment. If the results of FM1-43 uptake studies

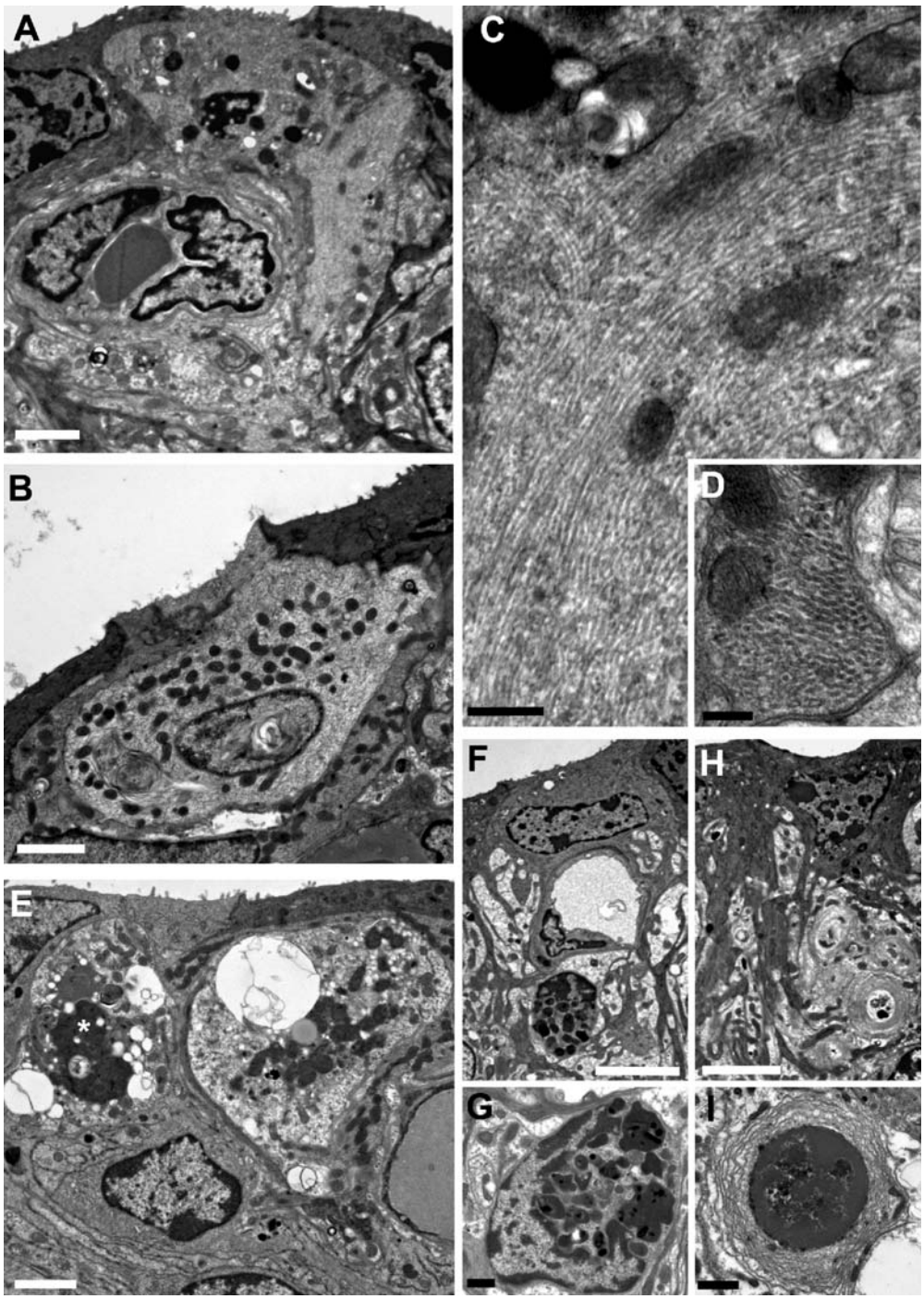

FIG. 9. **A** Marginal cell at 7 days posttreatment has much lighter cytoplasm than normal marginal cells, as evident in neighbors. The apex shows numerous small microvilli. Neighboring, more normal-appearing marginal cells appear to be extending processes to enclose the apex of the cell. Condensed chromatin in the nucleus and apparent fragmentation suggests apoptosis, but mitochondria appear mainly intact. *Scale bar*, 5 μm. **B** Marginal cell with light cytoplasm at 14 days posttreatment is rounding up and contains membranous whorls in the cytoplasm and in the nucleus, indicating degeneration, but mitochondria again appear intact. Microvilli at the cell surface. *Scale bar*, 2 μm. **C** Cytoplasm of a marginal cell with lighter cytoplasm (higher power of cell at 7 days posttreatment in **A**) is filled with parallel filaments ca. 20–5 nm wide reminiscent of microtubules. *Scale bar*, 0.5 μm. **D** Filamentous structures at the basal end of a marginal cell (2 weeks posttreatment) cut transversally with microtubule-like appearance. *Scale bar*, 0.2 μm. **E** Marginal cells enclosed within the epithelium at 2 weeks posttreatment. In the cell to the left, the nucleus marked with an *asterisk* shows condensed chromatin suggesting apoptosis. Many of the mitochondria in the degenerating cells, of a size consistent with those of marginal cells, are intact. *Scale bar*, 2 μm. **F**, **G** Electron dense inclusions in stria at 2 weeks posttreatment. Inclusions at the approximate level of the intermediate cells (**F**) are inside cells in which the nucleus is intact (**G**), suggesting that cellular debris is being cleared. **H**, **I** Cellular degeneration in stria (2 weeks posttreatment). Cell debris enclosed within the membranous whorls in the body of the stria, suggesting clearance of dying cells within the epithelium. *Scale bars*, 5 μm (**H**); 0.5 μm (**I**).

are a reasonable measure of aminoglycoside entry, then the drug may be at high levels in hair cells by 6 h posttreatment, a time compatible with the loss of OHC in most of the basal coil by 18 h.

OHC death

The morphology of nuclei labeled with DAPI or propidium iodide and seen in thin sections confirmed that OHC were dying via programmed cell death. The presence of TUNEL-positive nuclei and the identification of activated caspase-3 suggests that the "classical" caspase-dependent apoptotic pathway was triggered, at least in OHC, in response to the ototoxic damage. This supports a previous observation of activation of caspase-3 during OHC death in vivo following a chronic amikacin treatment regime in juvenile rats (Ladrech et al. 2004). In contrast, in a previous study of OHC loss following chronic treatment of mature mice with kanamycin alone over a 14-day period, neither TUNEL- nor activated caspase-3-positive OHC could be detected during the period of several days following treatment over which OHC died (Jiang et al. 2006). The evidence presented there suggested that, following aminoglycoside-induced injury to the mature organ of Corti in vivo, OHC die by caspase-independent apoptotic pathways. One difference between that work and the present one (in addition to the exposure of animals to bumetanide) is in the different timing of the onset and progression of injury; that is, between a chronic condition and acute hair cell loss. During the rapidly progressive hair cell death that is initiated following noise trauma in the mature organ of Corti in vivo, both TUNEL-positive nuclei and caspase-3 activation have been identified (Hu et al. 2002; Nicotera et al. 2003; Hu et al. 2006; Jiang et al. 2006). Caspase activation appears also to be involved in the acute aminoglycoside-induced apoptotic death of hair cells in explant cultures of the avian basilar papilla (Cheng et al. 2003) and the utricular maculae of birds (Matsui et al. 2002, 2004) and of mammals (Forge and Li 2000; Cunningham et al. 2002). The basis of a difference in hair cell death pathways between chronic and acute aminoglycoside exposure conditions in vivo is, however, difficult to explain. Differences in routes of drug entry and, thus, access to different cellular compartments, in rate of accumulation of aminoglycoside inside the cell, in the level and nature of damaging free radicals that are released, or some combination of those might be involved.

However, the present results do not rule out the existence of caspase-independent routes of hair cell death under the conditions used. As Ladrech et al. (2004) also found, not all OHC that showed apoptotic nuclei labeled for activated caspase-3 and the number of such positively labeled cells was relatively small. This may indicate that, whereas some cells are triggered to die via the classical apoptotic route, other cells are subjected to alternative signals leading to an apoptotic death by caspase-independent pathways (Jiang et al. 2006). Alternatively, it may be that only a small number of cells label for activated caspase-3 either because the activated enzyme is expressed only transiently or rupture of apoptotic OHC through a secondary necrosis (discussed below) occurs soon after the activation of caspase-3 such that the enzyme, along with other soluble cytoplasmic components, are released into, and become dissipated within, the fluid spaces of the organ of Corti.

Necrosis amongst OHC was almost completely undetectable. The presence of cellular debris closely associated with condensed apoptotic-like nuclei in regions of ongoing OHC death, observed both in sections and whole mounts, is, thus, most likely due to OHC entering the apoptotic pathway but failing to complete it. An as-yet undocumented death pathway may be involved, but it would be more reasonable to assume that apoptosis was initiated and then, before total shrinkage of the cell had occurred, the plasma membrane burst to release cell contents within the epithelium. In other systems it has been found that cells activating an apoptotic program may undergo "secondary necrosis" and rupture, especially under conditions in which phagocytosis of the apoptotic cell is delayed (Kelly et al. 1999; Wiegand et al. 2001). In the organ of Corti, supporting cells appear to have a role in clearing the dying hair cells (Abrashkin et al. 2006), and in mammalian vestibular organs, supporting cells phagocytose the intact apoptotic bodies of hair cells (Li and Forge 1995; Li et al. 1995; Forge and Li 2000). However, the specialized architecture of the organ of Corti may impede the ability of Deiters' cells to efficiently phagocytose the apoptotic bodies of the hair cells, with the consequence that secondary necrosis ensues.

IHC death and survival

IHC death, when it occurred, always succeeded loss of all OHC, and IHC often persisted for prolonged periods after all OHC had disappeared from the entire length of the organ of Corti. This suggests a pronounced differential sensitivity to damage between OHC and IHC. In other mammals, including humans (Wright et al. 1987), IHC loss is delayed, and less extensive, relative to loss of OHC, but it is usually found that IHC loss soon follows significant OHC loss and is initiated while OHC not far from the site of IHC death in the same cochlea are still present. The marked difference in damage sensitivity between OHC and IHC that was observed was not a kanamycin-specific phenomenon; the same pattern of hair cell loss was observed when either amikacin or gentamicin was administered instead of kanamycin. The continued presence of IHC

when all OHC have been lost has also been observed in mice after chronic kanamycin treatment (Forge et al., unpublished manuscript), suggesting that the differential sensitivity between OHC and IHC is not related to treatment conditions and how quickly OHC die. Prolonged survival of IHC after extensive loss of OHC is also evident in mice with certain genetic defects that lead to hair cell loss. For example, in mice lacking the Kcc4 cotransporter, IHC persist when all OHC are lost and may survive for several months (Boettger et al. 2002), and in Barhl1-deficient mice, while OHC are completely lost by postnatal day 59, IHC may still be present at 6 months (Li et al. 2002). These observations suggest that, in mice, IHC maybe particularly, and unusually, resistant to damage. This may have implications for the use of mice as models for human deafness. Nonetheless, the clear temporal separation between death of OHC from death of IHC that is exposed by the protocol described here provides opportunities to examine the factors that induce death of IHC and of possible intervention strategies to prevent it.

An aminoglycoside can persist in inner ear fluids, both perilymph and endolymph, for a long time after it has been cleared from serum (Harpur and Gonda 1982; Tran Ba Huy et al. 1986). The delay in IHC death commonly observed following aminoglycoside exposure could be attributable to persistence of drug in cochlear fluids leading to continuing uptake into IHC over a prolonged period until a critical level necessary to initiate damage is reached. However, in the present study, the single doses of drugs used were sufficient to cause rapid death of apical coil OHC. In other species, OHC in the apical coil are relatively less vulnerable to damage than those in the basal coil, and they may persist even when basal coil IHC have been lost. The results of the present study thus suggest a significant resistance of IHC to damage.

A second reason proposed for the relative resistance of IHC in comparison with OHC is differences in the extent of uptake of aminoglycosides between OHC and IHC. As pointed out above, several pieces of evidence suggest aminoglycosides can enter hair cells via the transduction channel (Gale et al. 2001; Meyers et al. 2003; Marcotti et al. 2005; Waguespack and Ricci 2005). The probability of the open state of the transduction channel is greatest for OHC in the basal coil and least for IHC (Gale et al. 2001). Thus, aminoglycosides may enter basal coil OHC most readily and IHC least. However, the experiments exploring the uptake of FM1-43 demonstrated that the dye entered IHC at least as readily as OHC both in vitro and in vivo in the mature organ of Corti, a finding for the in vivo condition in agreement with that of Meyers et al. (2003). This might suggest that differential uptake of aminoglycoside between OHC and IHC cannot account for the prolonged persistence of IHC in the absence of all OHC. It is important to stress that the experiments were not designed to test whether FM1-43 entered hair cells via the transduction channels or by endocytotic activity, although in the in vitro experiments the latter pathway would be restricted by the short (10 s) exposure of the cells to the dye, and by immediate transfer to cold buffer. Rather, the experiments tested merely whether there was differential uptake of FM1-43 between OHC and IHC. Nevertheless, if FM1-43 is a legitimate model of aminoglycoside uptake, then differential resistance between IHC and OHC in the kanamycin–bumetanide-treated mice cannot be explained by differential uptake of the drug. Furthermore, if entry of FM1-43 into IHC indicates that aminoglycoside can enter readily, then the survival of IHC for prolonged periods would imply that IHC have an inherent resistance to damage.

In organotypic cultures of explants of very early postnatal organ of Corti taken from animals at P1 or P2, direct exposure to gentamicin causes loss of IHC at least as early, if not preceding, initial loss of OHC (Camp et al., unpublished manuscript). However, in explants taken from slightly older animals, IHC appear relatively more resistant to aminoglycoside-induced death (Richardson et al. 1997). This might suggest that IHC develop resistance as they mature. Investigation of the molecular characteristics of very early postnatal IHC in comparison with those of older animals may provide clues as to particular survival factors expressed by IHC that underlie their resistance to ototoxic damage. Moreover, this present model in which death of IHC is significantly delayed with respect to that of OHC offers opportunities to explore factors underlying hair cell survival in vivo in the mature organ of Corti.

Also, if our interpretation is correct, then the death of IHC when it occurs may not be directly related to the toxic effects of the drugs but be a secondary phenomenon triggered by factors other than and different from those that initiate OHC death. This may have implications for therapeutic interventions aimed at preventing hair cell loss. Several modes of cell death may be at play during loss of IHC. Apoptotic death of IHC has been demonstrated in juvenile rats treated chronically with amikacin (Lenoir et al. 1999). Both the occurrence of TUNEL-positive IHC nuclei and nuclear morphology in thin sections as observed in the present study confirm in mice that apoptosis is a mode of IHC death following ototoxin-induced damage to the organ of Corti. However, there were also a few IHC that appeared to be necrotic. In addition, there were cells that showed a number of features suggesting they were involved in degeneration of their own cellular material: internalization of the stereocilia and/or the presence of cytoplasmic material and cell organelles enclosed within vacuoles, some of which were double-membraned,

a feature described as characteristic of autophagy (Eskelinen 2005; Reggiori and Klionsky 2005).

Autophagy is a mechanism for turnover and recycling of cell components through the lysosomes. It is meant to promote cell survival and protection from damage and is often triggered in response to conditions of stress, including starvation (Debnath et al. 2005; Reggiori and Klionsky 2005). However, autophagy may also be a programmed cell death pathway, which is sometimes called type II cell death. Accumulation of autophagic vesicles in cells is seen in a number of neurodegenerative diseases (Cuervo 2004; Lockshin and Zakeri 2004; Tsujimoto and Shimizu 2005). Autophagy may also be functionally linked to apoptosis: cells initiating autophagy may switch to apoptosis or vice versa (Cuervo 2004; Yousefi et al. 2006). While morphological features similar to autophagy-related cell death were seen in IHC in the present study, unfortunately, there are few specific markers that can be used for more objective immunohistochemical detection of autophagy in mammalian cells. Ultrastructural characteristics determined by electron microscopy are currently the usual means for its identification (Mizushima 2004; Martinet et al. 2006). Consequently, the interpretation that IHC may undergo autophagic degradation must be made cautiously.

Effects on the SV

The kanamycin–bumetanide treatment protocol not only caused extensive hair cell loss, but it also resulted in a significant thinning of the stria that was delayed in onset relative to OHC loss and progressively increased with time. The predominant site of injury appeared to be the marginal cells. The observed reduction in the basal infoldings of most marginal cells, and the apparent apoptotic death of some of them, appear to be characteristics of strial pathology following chronic aminoglycoside treatment (Forge et al. 1987), after noise trauma (Hirose and Liberman 2003) and with aging (Spicer and Schulte 2005). At a more detailed level, some of the abnormalities in marginal cells in the early stages of the progressive atrophy also resemble those described in the stria of aging gerbils (Spicer and Schulte 2005). That work reported stacked parallel clusters of thin processes that do not enclose mitochondria, similar to those identified in this study, as well as "thread-like structures" and "minivesicles" inside marginal cells, reminiscent of what has been defined here as microtubule-like filaments. At later stages of degeneration, there were aggregations of electron dense cellular inclusions, very similar to features in the stria of the aged mice, and which have been observed in the stria of aged gerbils and of noise-damaged mice (Hirose and Liberman 2003; Spicer and Schulte 2005). The similarities in the effects upon the stria across damage paradigms suggest common pathological events at the tissue and cellular level, although there may be differences in the factors that initiate those events. In the present work, damage to the stria was delayed relative to effects on the organ of Corti, and the thinning of the stria first became significant between 1 and 2 weeks posttreatment, coincident with the time of IHC loss. Inspection of the organ of Corti and SV in individual cochleae at the different time points also indicated that, in those cochleae where IHC persisted, the decrease of strial thickness was less than in those at the same posttreatment time where IHC were lost. It may be therefore that the initiation of damage in the stria is related to and follows from changes in ion homeostasis and physiological activity associated with the loss of hair cells. However, strial atrophy in the aging gerbil model appears to be independent of hair cell loss (Schulte and Schmiedt 1992), and in the noise-damaged mouse, in the basal cochlear coil where hair cell loss occurs, the stria appears unaffected (Hirose and Liberman 2003). Thus, effects on the stria may represent a separate damaging event, possibly unrelated to effects in the organ of Corti. Nevertheless, the present protocol may provide a means through which the triggering and progression of strial damage common to the different injuring agents, and of possible interventional strategies, can be examined at the cellular and molecular level applying the resources of various appropriate strains of mice.

A kanamycin–ethacrynic acid treatment protocol similar to that used here has been shown to have a comparable effect on the stria in guinea pigs (Hellier et al. 2002). That study found that, despite significant reduction in strial volume, EP is often maintained at near normal levels for prolonged periods after loss of hair cells. Likewise, EP is not affected significantly even after several weeks during the progressive strial atrophy that follows chronic, repeated aminoglycoside treatment, noise trauma and with aging (Komune and Snow 1982; Schulte and Schmiedt 1992; Hirose and Liberman 2003). It seems reasonable to assume, therefore, that, in the cochleae of mice with atrophying stria, EP is likely to be at close to normal levels and may be sufficient to maintain homeostasis in the changed physiological environment when there are no hair cells. However, in aging gerbils, continuing reduction in strial volume eventually leads to loss of EP (Schulte and Schmiedt 1992). In the present work, in some of the animals taken at 8–14 weeks posttreatment, the extent of strial atrophy was so marked that the normal cellular architecture was difficult to discern, and strial thickness was close to one third normal, a level at which it is said maintenance of EP is no longer possible (Schulte and Schmiedt 1992). It may be, therefore, that the progressive atrophy of the stria in these damaged mouse cochleae may continue

to the extent that a condition similar to that in aged gerbils is reached.

Findings, such as those reported here, that there maybe significant effects upon the stria and hair cell loss with different damaging agents has, of course, implications for any hair cell regenerative or replacement therapies that may evolve to ameliorate hearing impairment. The replacement hair cells must have an environment appropriate for their survival and proper functioning. Damage to the stria and to lateral wall fibrocytes, which maybe a primary site of injury with aging (Schulte and Schmiedt 1992; Hequembourg and Liberman 2001) and after noise trauma (Wang et al. 2002), are likely to cause changes in cochlear homeostasis that may well result in an environment unsuitable for the survival of the replacement hair cells. Greater understanding of the pathological processes in the nonsensory tissues of the cochlea, of the ways in which the cochlear environment changes when hair cells die, and of how those might be manipulated is required. The procedure presented in this paper may offer opportunities to address these issues in a variety of mouse models.

ACKNOWLEDGMENTS

This work was supported by a project grant from The Royal National Institute for Deaf People (RNID).

REFERENCES

ABRASHKIN KA, IZUMIKAWA M, MIYAZAWA T, WANG CH, CRUMLING MA, SWIDERSKI DL, BEYER LA, GONG TW, RAPHAEL Y. The fate of outer hair cells after acoustic or ototoxic insults. Hear. Res. 218:20–29, 2006.

BOETTGER T, HUBNER CA, MAIER H, RUST MB, BECK FX, JENTSCH TJ. Deafness and renal tubular acidosis in mice lacking the K–Cl co-transporter Kcc4. Nature 416:874–878, 2002.

BRUMMETT RE, BENDRICK T, HIMES D. Comparative ototoxicity of bumetanide and furosemide when used in combination with kanamycin. J. Clin. Pharmacol. 21:628–636, 1981.

CHENG AG, CUNNINGHAM LL, RUBEL EW. Hair cell death in the avian basilar papilla: characterization of the *in vitro* model and caspase activation. J. Assoc. Res. Otolaryngol. 4:91–105, 2003.

CUERVO AM. Autophagy: in sickness and in health. Trends Cell Biol. 14:70–77, 2004.

CUNNINGHAM LL, CHENG AG, RUBEL EW. Caspase activation in hair cells of the mouse utricle exposed to neomycin. J. Neurosci. 22:8532–8540, 2002.

DAVIES S, FORGE A. Preparation of the mammalian organ of Corti for scanning electron microscopy. J. Microsc. 147:89–101, 1987.

DEBNATH J, BAEHRECKE EH, KROEMER G. Does autophagy contribute to cell death? Autophagy 1:66–74, 2005.

ESKELINEN EL. Maturation of autophagic vacuoles in Mammalian cells. Autophagy 1:1–10, 2005.

FORGE A. Outer hair cell loss and supporting cell expansion following chronic gentamicin treatment. Hear. Res. 19:171–182, 1985.

FORGE A, LI L. Apoptotic death of hair cells in mammalian vestibular sensory epithelia. Hear. Res. 139:97–115, 2000.

FORGE A, SCHACHT J. Aminoglycoside antibiotics. Audiol. Neurootol. 5:3–22, 2000.

FORGE A, WRIGHT A, DAVIES SJ. Analysis of structural changes in the stria vascularis following chronic gentamicin treatment. Hear. Res. 31:253–265, 1987.

GALE JE, MARCOTTI W, KENNEDY HJ, KROS CJ, RICHARDSON GP. FM1-43 dye behaves as a permeant blocker of the hair-cell mechanotransducer channel. J. Neurosci. 21:7013–7025, 2001.

GRIESINGER CB, RICHARDS CD, ASHMORE JF. Fm1-43 reveals membrane recycling in adult inner hair cells of the mammalian cochlea. J. Neurosci. 22:3939–3952, 2002.

HARPUR ES, GONDA I. Analysis of the phamacokinetics of ribostamycin in serum and perilymph of guinea pigs after single and multiple doses. Br. J. Audiol. 16:95–99, 1982.

HELLIER WP, WAGSTAFF SA, O'LEARY SJ, SHEPHERD RK. Functional and morphological response of the stria vascularis following a sensorineural hearing loss. Hear. Res. 172:127–136, 2002.

HEQUEMBOURG S, LIBERMAN MC. Spiral ligament pathology: a major aspect of age-related cochlear degeneration in C57BL/6 mice. J. Assoc. Res. Otolaryngol. 2:118–129, 2001.

HIROSE K, LIBERMAN MC. Lateral wall histopathology and endocochlear potential in the noise-damaged mouse cochlea. J. Assoc. Res. Otolaryngol. 4:339–352, 2003.

HU BH, HENDERSON D, NICOTERA TM. Involvement of apoptosis in progression of cochlear lesion following exposure to intense noise. Hear. Res. 166:62–71, 2002.

HU BH, HENDERSON D, NICOTERA TM. Extremely rapid induction of outer hair cell apoptosis in the chinchilla cochlea following exposure to impulse noise. Hear. Res. 211:16–25, 2006.

IZUMIKAWA M, MINODA R, KAWAMOTO K, ABRASHKIN KA, SWIDERSKI DL, DOLAN DF, BROUGH DE, RAPHAEL Y. Auditory hair cell replacement and hearing improvement by Atoh1 gene therapy in deaf mammals. Nat. Med. 11:271–276, 2005.

JIANG H, SHA SH, FORGE A, SCHACHT J. Caspase-independent pathways of hair cell death induced by kanamycin *in vivo*. Cell Death Differ. 13:20–30, 2006.

KELLY L, REID L, WALKER NI. Massive acinar cell apoptosis with secondary necrosis, origin of ducts in atrophic lobules and failure to regenerate in cyanohydroxybutene pancreatopathy in rats. Int. J. Exp. Pathol. 80:217–226, 1999.

KOMUNE S, SNOW JB, JR. Nature of the endocochlear dc potential in kanamycin-poisoned guinea pigs. Arch. Otolaryngol. 108:334–338, 1982.

LADRECH S, GUITTON M, SAIDO T, LENOIR M. Calpain activity in the amikacin-damaged rat cochlea. J. Comp. Neurol. 477:149–160, 2004.

LADRECH S, WANG J, SIMONNEAU L, PUEL JL, LENOIR M. Macrophage contribution to the response of the rat organ of Corti to amikacin. J. Neurosci. Res. 85:1970–1979, 2007.

LENOIR M, DAUDET N, HUMBERT G, RENARD N, GALLEGO M, PUJOL R, EYBALIN M, VAGO P. Morphological and molecular changes in the inner hair cell region of the rat cochlea after amikacin treatment. J. Neurocytol. 28:925–937, 1999.

LI L, FORGE A. Cultured explants of the vestibular sesnory epithelia from adult guinea pigs and effects of gentamcin: a model for examination of hair cell loss and epithelial repair mechanisms. Audit. Neurosci. 1:111–125, 1995.

LI L, NEVILL G, FORGE A. Two modes of hair cell loss from the vestibular sensory epithelia of the guinea pig inner ear. J. Comp. Neurol. 355:405–417, 1995.

LI S, PRICE SM, CAHILL H, RYUGO DK, SHEN MM, XIANG M. Hearing loss caused by progressive degeneration of cochlear hair cells in mice deficient for the Barhl1 homeobox gene. Development 129:3523–3532, 2002.

LOCKSHIN RA, ZAKERI Z. Apoptosis, autophagy, and more. Int. J. Biochem. Cell Biol. 36:2405–2419, 2004.

MARCOTTI W, VAN NETTEN SM, KROS CJ. The aminoglycoside antibiotic dihydrostreptomycin rapidly enters mouse outer hair cells through the mechano-electrical transducer channels. J. Physiol. 567:505–521, 2005.

MARTINET W, DE MEYER GR, ANDRIES L, HERMAN AG, KOCKX MM. Detection of autophagy in tissue by standard immunohistochemistry: possibilities and limitations. Autophagy 2:55–57, 2006.

MATSUI JI, OGILVIE JM, WARCHOL ME. Inhibition of caspases prevents ototoxic and ongoing hair cell death. J. Neurosci. 22:1218–1227, 2002.

MATSUI JI, GALE JE, WARCHOL ME. Critical signaling events during the aminoglycoside-induced death of sensory hair cells *in vitro*. J. Neurobiol. 61:250–266, 2004.

MCFADDEN SL, DING D, JIANG H, WOO JM, SALVI RJ. Chinchilla models of selective cochlear hair cell loss. Hear. Res. 174:230–238, 2002.

MEYERS JR, MACDONALD RB, DUGGAN A, LENZI D, STANDAERT DG, CORWIN JT, COREY DP. Lighting up the senses: FM1-43 loading of sensory cells through nonselective ion channels. J. Neurosci. 23:4054–4065, 2003.

MIZUSHIMA N. Methods for monitoring autophagy. Int. J. Biochem. Cell Biol. 36:2491–2502, 2004.

NICOTERA TM, HU BH, HENDERSON D. The caspase pathway in noise-induced apoptosis of the chinchilla cochlea. J. Assoc. Res. Otolaryngol. 4:466–477, 2003.

PRIEVE BA, YANZ JL. Age-dependent changes in susceptibility to ototoxic hearing loss. Acta. Otolaryngol. 98:428–438, 1984.

RAPHAEL Y, ALTSCHULER RA. Scar formation after drug-induced cochlear insult. Hear. Res. 51:173–183, 1991.

REGGIORI F, KLIONSKY DJ. Autophagosomes: biogenesis from scratch? Curr. Opin. Cell. Biol. 17:415–422, 2005.

RICHARDSON GP, FORGE A, KROS CJ, FLEMING J, BROWN SD, STEEL KP. Myosin VIIA is required for aminoglycoside accumulation in cochlear hair cells. J. Neurosci. 17:9506–9519, 1997.

RUSSELL NJ, FOX KE, BRUMMETT RE. Ototoxic effects of the interaction between kanamycin and ethacrynic acid. Cochlear ultrastructure correlated with cochlear potentials and kanamycin levels. Acta Otolaryngol. 88:369–381, 1979.

SANTI PA, DUVALL AJ, 3RD. Morphological alteration of the stria vascularis after administration of the diuretic bumetanide. Acta Otolaryngol. 88:1–12, 1979.

SCHULTE BA, SCHMIEDT RA. Lateral wall Na, K-ATPase and endocochlear potentials decline with age in quiet-reared gerbils. Hear. Res. 61:35–46, 1992.

SPICER SS, SCHULTE BA. Pathologic changes of presbycusis begin in secondary processes and spread to primary processes of strial marginal cells. Hear. Res. 205:225–240, 2005.

TRAN BA HUY P, MEULEMANS A, MANUEL C, STERKERS O, WASSEF M. Critical appraisal of the experimental studies on the ototoxic interaction between ethacrynic acid and aminoglycoside antibiotics. A pharmacokinetical standpoint. Scand. Audiol. Suppl. Suppl. 14:225–232, 1981.

TRAN BA HUY P, BERNARD P, SCHACHT J. Kinetics of gentamicin uptake and release in the rat. Comparison of inner ear tissues and fluids with other organs. J. Clin. Invest. 77:1492–1500, 1986.

TSUJIMOTO Y, SHIMIZU S. Another way to die: autophagic programmed cell death. Cell Death Differ. 12(Suppl 2):1528–1534, 2005.

WAGUESPACK JR, RICCI AJ. Aminoglycoside ototoxicity: permeant drugs cause permanent hair cell loss. J. Physiol. 567:359–360, 2005.

WANG Y, HIROSE K, LIBERMAN MC. Dynamics of noise-induced cellular injury and repair in the mouse cochlea. J. Assoc. Res. Otolaryngol. 3:248–268, 2002.

WEBER T, ZIMMERMANN U, WINTER H, MACK A, KÖPSCHALL I, ROHBOCK K, ZENNER HP, KNIPPER M. Thyroid hormone is a critical determinant for the regulation of the cochlear motor protein prestin. Proc. Natl. Acad. Sci. U. S. A. 99:2901–2906, 2002.

WEBSTER M, WEBSTER DB. Spiral ganglion neuron loss following organ of Corti loss: a quantitative study. Brain Res. 212:17–30, 1981.

WEST BA, BRUMMETT RE, HIMES DL. Interaction of kanamycin and ethacrynic acid. Severe cochlear damage in guinea pigs. Arch Otolaryngol. 98:32–37, 1973.

WIEGAND UK, CORBACH S, PRESCOTT AR, SAVILL J, SPRUCE BA. The trigger to cell death determines the efficiency with which dying cells are cleared by neighbours. Cell Death Differ. 8:734–746, 2001.

WRIGHT A, DAVIS A, BREDBERG G, ULEHLOVA L, SPENCER H. Hair cell distributions in the normal human cochlea. Acta Otolaryngol. Suppl. 444:1–48, 1987.

WU WJ, SHA SH, MCLAREN JD, KAWAMOTO K, RAPHAEL Y, SCHACHT J. Aminoglycoside ototoxicity in adult CBA, C57BL and BALB mice and the Sprague–Dawley rat. Hear. Res. 158:165–178, 2001.

YOUSEFI S, PEROZZO R, SCHMID I, ZIEMIECKI A, SCHAFFNER T, SCAPOZZA L, BRUNNER T, SIMON HU. Calpain-mediated cleavage of Atg5 switches autophagy to apoptosis. Nat. Cell Biol. 8:1124–1132, 2006.